SUSPENDED SAND CONCENTRATION MODELS UNDER BREAKING WAVES: EVALUATION OF NEW AND EXISTING FORMULATIONS

First Author: Gabriel Lim[a]
Second (Corresponding) Author: Ravindra Jayaratne[b*]
Third Author: Tomoya Shibayama[c]

[a,b]University of East London, Docklands Campus, University Way, E16 2RD, London, UK. [a]g.lim@uel.ac.uk, [b]r.jayaratne@uel.ac.uk
[c]Waseda University, 3-4-1 Ookubo, Shinjuku-ku, Tokyo, Japan. [c]shibayama@waseda.jp

Declarations of Interest: None

ABSTRACT

A total of 7 reference concentration (C_0) models (6 existing and 1 newly proposed) were validated against 119 test cases from 4 recently published datasets collected under the *LIP*, *CROSSTEX*, *SandT-Pro* and *SINBAD* experimental studies. These models were evaluated for performance in different cross-shore regions: the shoaling zone, breaking (outer surf) zone and inner surf zone, under regular and irregular breaking wave conditions. In almost all existing C_0 models, substantial under-prediction was found particularly around the wave plunging point (point at which breaking wave plunges and surface generated turbulent kinetic energy, TKE, is injected into the water column) where strong localised increases in C_0 were observed. This strong increase in concentration was attributed to the large-scale breaking-generated turbulent vortices invading the wave bottom boundary layer (WBBL) and entraining dense clouds of sediment near the plunging point. Models that were directly or indirectly driven by local wave climate such as the wave height (H), breaker height (H_b) or local water depth (d), were found to perform quite poorly in the breaking region under regular and irregular plunging breaker waves. Formulations that related C_0 to the sand pickup rate (i.e. depending on exerted bed shear exceeding critical bed shear for entrainment) were adept in regions unaffected by external breaking-induced TKE (e.g. the shoaling zone) but could not account for the high levels of concentration observed at the plunging point. This is because these formulations were based on the implicit assumption that sediment entrainment is only induced by the local TKE generated by bed shear; not taking surface-generated breaking-induced TKE into account. This assumption was addressed in more recent studies, by including breaking-induced TKE into sediment pickup rate or reference concentration formulations. Though latest studies have shown promising relationships between near-bed TKE (k_b) and reference concentration/sediment pickup, such formulations also face inherent limitations. These formulations are highly dependent on the accuracy of measured or modelled k_b and are also sensitive to the magnitude of k_b. For example, the magnitude of measured k_b was found to vary by a factor of 1.1-1.3 between regular and irregular wave conditions, with k_b being smaller under irregular wave conditions. This resulted in varied performance between datasets in k_b-driven reference concentration formulations. The Froude-scaled TKE produced smaller deviations in magnitude of TKE between datasets, suggesting that it may be a more suitable driving parameter for reference concentration models than k_b. A new reference concentration model, L19, was empirically derived from an inverse relationship observed between d and C_0, and from the roller energy dissipation rate. The newly proposed L19 model shows good agreement with measured C_0 (with RMSE ranging between 0.36-1.79kg/m^3 over the different datasets) in regular and irregular wave conditions, even at the plunging point where concentration is highest. The modified concentration profile [$C(z)$] equation also performs well, generally capturing the vertical concentration profile accurately throughout the whole water column.

Keywords: reference concentration, suspended sand concentration, breaking waves, numerical modelling, near-shore, turbulent kinetic energy

1. Introduction

Over the years, experimental studies have reported that the magnitude of sediment suspension (e.g. Kana 1978, 1979; Shibayama & Rattanapitikon, 1993; Beach & Sternberg, 1996; Voulgaris & Collins, 2000), turbulence production and transport mechanisms (Ting & Kirby, 1994; van der Zanden et al., 2016, henceforth abbreviated to vdZ et al. 2016) found within the surf zone are a function of the wave type. Under non-breaking wave conditions, the suspended sediment concentration is largely confined to the thin layer above the bottom, known as the wave bottom boundary layer (referred to as WBBL or WBL in existing literature). This however is not the case under breaking conditions, where the sediment is suspended over the whole water column. Considerable differences can also be observed in the concentration profile and turbulence structure (Brinkkemper et al., 2016) depending on the breaker types.

Yoon & Cox (2010) reported that the time-scale of turbulence propagation was relatively longer under spilling breakers, with corresponding turbulence intensities being relatively constant at any given time due to advection of residual turbulence from previous breakers. This is consistent with the observations of Brinkkemper et al. (2016) who found that the amount of turbulence measured was homogenous over the whole wave cycle under spilling breakers. Aagaard et al. (2018) also reported near-bed turbulence under spilling breakers peaking much later in the wave cycle, suggesting slower penetration of surface-generated turbulent kinetic energy (TKE) into the water column. It is speculated that this may be a result of turbulence in spilling breakers being largely confined in the upper water column due to relatively small eddies present under these conditions (c.f. Brinkkemper et al., 2016). On the contrary, TKE under plunging breakers is generated almost immediately after the wave has broken (Ting & Kirby, 1995). A large amount of the breaking-generated TKE is dissipated in the form of bores above the water surface, and the remainder is injected into the water column (vdZ et al. 2016). As the waves plunge, a jet (Shibayama & Rattanapitikon, 1993) of highly pressurised (Mocke & Smith, 1992) and aerated water (Voulgaris and Collins, 2000; Yoon and Cox, 2010) is thrust into the water column at the plunging point. This plunging process generates strong turbulent vortices (vdZ et al. 2016; 2018; Aagaard et al., 2018) that rotate about the horizontal axis (Aagaard & Hughes, 2010). These vortices travel rapidly (vdZ et al., 2017a) and obliquely downwards towards the bed (Nadaoka et al., 1989; Brinkkemper et al., 2016) and shoreward in the direction of wave propagation (Peregrine & Svendsen, 1978). Turbulent kinetic energy is dissipated as it travels down the water column, from the surface to the bed. Despite the turbulence dissipation throughout the water column, varying amounts of TKE can still reach the bed (Grasso et al., 2012), transported by the large-scale eddies (Ting & Kirby, 1995). Especially in regions where the water depth is shallow, the externally injected TKE can contribute significantly to the near-bed TKE (Scott et al., 2005; vdZ et al. 2016). As the turbulent vortices reach the bed, the external turbulence adds to the locally produced TKE induced by bed shear (Sumer et al., 2013) in the WBBL. Though not the dominant source of TKE in the surf zone, turbulence induced by bed shear can also contribute importantly to near-bed TKE (Brinkkemper et al., 2016; vdZ et al. 2016).

As the highly turbulent large-scale vortices invade the WBBL, they can entrain large amounts of sediment from the bed (Aagaard & Hughes, 2010; vdZ et al. 2017a) in the form of dense clouds (Sato et al., 1990, Shibayama & Rattanapitikon, 1993). The breaking-generated TKE does not only travel vertically (injection, dissipation, vertical advection and diffusion), but is also advected horizontally in the offshore direction (vdZ et al. 2016). The dense clouds of sediment can also be advected away from the breaking/plunging point and contribute to net sediment transport (Aagaard & Hughes, 2010) and increase concentration in adjacent cross-shore regions. This breaking-induced turbulence does not decay entirely within one wave cycle and can linger in the breaker bar trough region as 'residual turbulence' (Fernandez-Mora et al., 2016; vdZ et al. 2016; van der A et al., 2017). Trapped air bubbles from the plunger also rise towards the surface (Ting & Kirby, 1995; Mori et al., 2007; Jayaratne & Shibayama, 2007) generating large upwards-localised velocities (Voulgaris & Collins, 2000), which carry suspended sediment into the upper water column. The combination of the rising air bubbles and the highly turbulent vortices enhances strong vertical sediment mixing in the breaking region (Nielsen, 1984; Ogston & Sternberg, 2002; Aagaard & Hughes, 2010; Aagaard & Jensen, 2013; Yoon *et al.*, 2015).

In recent years, various experimental and numerical studies have enhanced our understanding of such processes, providing valuable insights into once poorly understood physical phenomena such as wave breaking and the complex interactions between the resulting hydrodynamics and local sediment. However, even with novel insights, describing the complex sediment movement within the surf zone is still difficult, as it is influenced by cross-shore hydrodynamic non-uniformity (van Rijn et al., 2013; vdZ et al. 2017a), breaking induced turbulence and asymmetric oscillatory motion under shallow water waves (Sato et al., 1990). A considerable number of studies have endeavoured to model the suspended sand concentration (SSC) at a near-bottom reference level, i.e. reference concentration (C_0), as well as the vertical concentration profile [$C(z)$]. Some have related the reference concentration to the bed shear stress or bed shear velocity, or the dimensionless bed shear stress – i.e. Shields Parameter (e.g. Van Rijn, 1984, 2007; Shibayama & Rattanapitikon 1993; Camenen & Larson, 2008), others to local wave height, water depth or relative wave height (e.g. Mocke & Smith, 1992) or the wave height at the breaking point (e.g. Jayaratne & Shibayama, 2007), energy dissipation of the surface roller (e.g. Smith & Mocke, 1993; Spielmann et al., 2004), inclusion of

near-bed TKE to increase bed shear stress (e.g. Hsu & Liu, 2004; Okayasu et al., 2010; vdZ et al. 2017b) and formulations that incorporate near-bottom TKE as the main driving parameter (e.g. Yoon et al., 2015). The reference concentration is often used to compute the concentration profile, which in turn can be used to compute the (current-related) suspended load transport rate. As such, the performance (and improvement) of reference concentration and concentration profile models can have a direct impact on our ability to accurately reproduce sand transport rates and resulting morphodynamic changes. Small discrepancies between measured and computed suspended load can accumulate over time, leading to unrealistic predictions of resulting morphology, particularly in the medium- to long-term. The aim of the present study therefore is to validate and evaluate the performance of 7 (6 existing and 1 newly proposed) reference concentration models against 4 recently published datasets that were collected under regular and irregular large-scale breaking waves.

The models are introduced, and key parameters described in section 2 of this paper. Section 3 gives a brief description of the test conditions and relevant information regarding the datasets used to validate the models in this study. The datasets used are from '*LIP*' (refer to Roelvink & Reniers, 1995), '*CROSSTEX'* (refer to Yoon & Cox, 2010), '*SandT-Pro'* (refer to Ribberink et al., 2014) and '*SINBAD'* (refer to vdZ et al. 2016) projects. In section 4, the models (described in section 2) are then validated quantitatively and qualitatively against 119 test cases of data. A discussion of the findings from the model validation is presented in section 5 and finally section 6 provides an overview of the conclusions of this paper.

2. Model Formulation

It should be noted that in this section commonly used parameters such as the wave climate (e.g. wave height, length, period), local water depth and any other parameters used in multiple formulae are the same for all formulations unless specified otherwise. As such, any parameters that are defined in earlier formulae are not repeated for each new set of formulae unless there are variations in their definition.

2.1 Reference Concentration – C_0

Mocke & Smith (1992) – MS92

The reference concentration formula of Mocke & Smith (1992) was comprised of three main terms: the relative wave height term (which was a measure of breaking intensity and depth penetration), a turbulence dissipation term (based on periodic bores) and a TKE term (which incorporated TKE from mean bed shear). The complementing relative wave height term, which represents the injection of TKE into the water column, is combined with the turbulence dissipation term and the Shields parameter to incorporate local TKE.

Mocke & Smith (1992) proposed the following equation to compute the bottom reference concentration (C_0) in kg/m^3:

$$C_0 = \rho_s K^{-0.92} (H/d)^{3.32} (H^3/dT)^{-0.92} \theta^{0.37} \quad (1)$$

where
ρ_s is the density of sand (taken to be 2650 kg/m^3)
$K = 1.51\times10^3$ sm^{-2} is a proportionality constant related to the turbulence dissipation term
H is local wave height
d is local water depth
T is the wave period
θ is the Shields Parameter

The Shields Parameter was defined by the following:

$$\theta = \tau/(\rho_w(s-1)gD_{50}) \quad (2)$$

where τ is the dimensional shear stress = $0.5\rho_w f_w u_*^2$
ρ_w = density of seawater = 1025kg/m^3
s is the specific gravity = ρ_s/ρ_w
f_w is the dimensionless grain roughness friction factor = exp(5.213*[(r)/(A_b)^0.194]-5.977) – based on Swart, (1974).
A_b is the orbital radius and r=2.5D_{50} is the hydraulic roughness (Nielsen, 1986)
u_* = bed shear velocity (m/s)
g = gravitational acceleration = 9.81m/s^2
D_{50} is the average grain diameter

Shibayama & Rattanapitikon (1993) – SR93

SR93 proposed a simple set of formulae to predict the reference concentration under breaking wave and non-breaking wave conditions. They assumed that the reference concentration was a function of the maximum bed shear, sediment diameter and in the case of non-breaking waves, also ripple-height. For breaking wave conditions, SR93 proposed two different formulations of the Shields Parameter: one for plunging waves and one for all other breaker types. The formulations of Shields Parameter used by SR93 are defined as:

$\psi_b = \{u_* + 0.01\,[H^3 g(4Td)]^{1/3}\}^2/[(s\text{-}1)gD_{50}]$ for plunging waves (3a)
$\psi_b = \psi = 0.5 f_w u_b^2/(s\text{-}1)gD_{50}$ for other breaker types (3b)

where
$H^3g(4Td)$ is the rate of wave energy dissipation due to wave breaking
u_b is the maximum orbital velocity.

Shear velocity or maximum shear velocity is one of the key driving parameters in the reference concentration formulation of SR93. For cases where the maximum shear velocity cannot be obtained using measurements, SR93 defined maximum shear velocity as:

$u_* = \sqrt{(0.5 f_w u_b^2)}$ (4)

The maximum orbital velocity is also an important parameter in the formulation of SR93. As the reference level is typically in the WBBL, it is assumed in this study that the maximum orbital velocity (u_b) can be equated to the near-bottom velocity at the breaking point ($\hat{u}_b$).

$u_b \approx \hat{u}_b$ (5)

where $\hat{u}_b$ can be found from Eq.11, K = wave number and L is the wavelength estimated from linear wave theory. Alternatively, the orbital velocity can be computed from the linear wave theory. Based on the computed Shields Parameter, experimental observations and sediment and fluid characteristics, the following formula was derived for the reference concentration (C_0) in g/l:

$C_0 = 10/3\,[(\psi_b - 0.05)v] / \{\sqrt{[(s\text{-}1)g\,D_{50}]}100D_{50}\}$ (6)

where
reference level $r = z_0 = 100D_{50}$
v = kinematic viscosity = $1.17\text{x}10^{-6}$ m^2/s, and 0.05 is the critical value of Shields Parameter for threshold general movement of sand.
Note: as the units g/l are equal to kg/m^3 (i.e. 1 g/l = 1 kg/m^3), the reference concentration computed using the formulae of SR93 and also JS07 (described later in this section) are displayed in kg/m^3 for uniformity of units in the analysis presented in sections 4 and 5.

Spielmann et al. (2004) – SP04

Spielmann et al. (2004) reported that in the surf zone, wave breaking caused a downward horizontal transfer in momentum from the fluid above the wave trough, which in turn contributed to the driving force for mean flow. Spielmann et al. (2004) took this effect into consideration by incorporating shear stress at the water surface. This surface shear stress (τ_s) was related to the roller dissipation rate (D_r) by Deigaard & Fredsoe (1989):

$\tau_s = D_r/c$ (7)

where c = wave celerity = $\sqrt{(g \cdot d)}$

The parameterisation of Nairn et al. (1990) was used to model the roller dissipation rate as follows:

$D_r = 2\beta g\, E_r/c$ (8)

where
β = coefficient related to the wave steepness = 0.1

One of the key parameters used in determining the roller dissipation rate is the roller energy E_r. This parameter can be computed using different methods, but in the present study the formulation of Svendsen (1984) has been implemented due to its computational efficiency:

$$E_r = \rho_w A c^2 / 2L \qquad (9)$$

where
A = roller area = estimated empirically as $0.9H^2$ by Svendsen (1984).
L = wavelength was estimated using linear wave theory.

SP04 emphasised the effect the breaking roller had on surf zone hydrodynamics, particularly in the vicinity of breaker bars. For this reason, it was deemed important to include the surface shear stress induced by the breaking roller and in turn, to propose a parameterisation that is dependent on the Shields Parameter. Instead of the standard bed shear stress used in the Shields Parameter, SP04 used the sea-surface shear stress induced by the breaking roller (τ_s). Based on the modified Shields Parameter, the following reference concentration formulation was proposed in kg/m^3:

$$C_0 = \alpha_c \rho_s [D_r / (\rho_s - \rho_w) g D_{50} c]^3 \qquad (10)$$

where:
α_c = dimensionless term = 1x10^{-6}

Jayaratne & Shibayama (2007) – JS07

The reference concentration (C_0) formula of Jayaratne & Shibayama (2007) was derived from the time-averaged suspended sediment transport rate. The formulation was driven mainly by the wave climate (wave height, wavelength, celerity, etc.) and to a lesser extent, the sediment characteristics/interaction (average grain diameter, settling velocity, etc.). One of the key drivers in the JS07 model is based on the relationship between the near-bottom velocity at the breaking point ($\hat{u}_b$) and the particle settling velocity (w_s). Jayaratne & Shibayama (2007) considered $\hat{u}_b$ to represent the intensity of near-bottom turbulence at the breaking point, which would in theory entrain the sediment from the bed. The settling velocity (w_s) would represent the magnitude of the opposite force that causes entrained sediment to settle again. It was proposed that the relationship between the two parameters would be effective in modelling the SSC under breaking wave conditions. The near-bottom velocity at the breaking point ($\hat{u}_b$) is derived as follows:

$$\hat{u}_b = \pi H_b / T \sinh(K_b d_b) \qquad (11)$$

where the subscript b denotes at the breaking point, K_b is the wave number at the breaking point = $2\pi/L_b$.

The relationship proposed by Jayaratne & Shibayama (2007) for computing reference concentration in g/l at the reference level of $100D_{50}$ was defined as:

$$C_0 = 1.22 * 10^{-6}\, g T\, \hat{u}_b^{2.3} / w_s^{3.3} \qquad (12)$$

where
w_s = particle settling velocity

Note: Jayaratne & Shibayama (2007) reported 1.22*10^{-9} instead of *10^{-6}. This is because the units used in JS07 were centimetres, whereas herein metres are used.

Though the above formulation was derived for breaking conditions only, for the purpose of testing its applicability to adjacent cross-shore zones also, the wave height (H) was used in place of the breaker height (H_b) in this study. This was also done with the wavelength (L) being used instead of breaker length (L_b) and local water depth (d) instead of breaker depth (d_b). This is further discussed in section 5.1 of this report.

Van Rijn (2007) – VR07

Van Rijn (1984) reported that some of the main driving hydraulic parameters of suspended load were the particle settling velocity and the sediment diffusion coefficient. It was assumed, in particular, that the reference concentration at the bed was determined by particle diameter (D_*) and the transport parameter T_Φ.

$$D_* = D_{50}[(s\text{-}1)g/\nu^2]^{1/3} \qquad (13)$$

The particle diameter, also referred to as the dimensionless grain size, is a function of the average grain diameter and also hydraulic parameters such as the kinematic viscosity (ν). The transport parameter is a dimensionless bed shear stress term that considers the induced bed shear velocity and the critical bed shear velocity, with the assumption that sediment movement occurs when the critical velocity is exceeded. The transport parameter T_Φ was modified in van Rijn (2007) to incorporate the current and wave related bed shear stress ($\tau'_{b,cw}$) and the Shields critical bed shear stress ($\tau'_{b,cr}$) instead of the bed shear velocity.

$$T_\Phi = (\tau'_{b,cw} - \tau'_{b,cr})/\tau'_{b,cr} \qquad (14)$$

$\tau'_{b,cr}$ = Shields critical bed shear stress
$\tau'_{b,cw}$ = current and wave related bed shear stress = $\tau'_{b,c} + \tau'_{b,w}$
$\tau'_{b,c}$ = current related bed shear stress and $\tau'_{b,w}$ = wave related bed shear stress
See van Rijn (2007) for details on how to derive the bed shear stresses.

For instantaneous volumetric reference concentration for suspended load, the following formula was proposed:

$$C_0 = 0.015 * D_{50}/a * T_\Phi^{1.5}/D_*^{0.3} \qquad (15)$$

a = the reference level, with minimum value of 0.01m. See van Rijn (2007) for details on deriving a. The minimum value of a = 0.01m is used in this study. Note: equation 15 gives the volumetric concentration and should therefore be multiplied by ρ_s =2650kg/m^3 to obtain C_0 in kg/m^3. Also, the model of van Rijn (2007) was only validated against the SINBAD and CROSSTEX datasets in this study. The reason for this is the measured wave orbital velocity (computed from measured rms wave orbital velocity) was not collected in the SandT-Pro experiments, and the time-averaged current velocity was not measured in the LIP experiments – both of these measurements are required as input parameters for VR07.

Van der Zanden et al. (2017b) – VZ17

The reference concentration C_0 equation is the same as that of van Rijn (1984; 2007), as is the reference level. The fundamental difference is in the inclusion of external breaking generated TKE into the transport parameter (T_Φ) of van Rijn (1984). The original transport parameter of van Rijn (1984) was proportionate to the sediment pick-up rate and represented the difference between exerted and critical bed shear. The transport parameter of van Rijn (1984) was as follows:

$$T_\Phi = (u_*^2 - u_{*cr}^2)/u_{*cr}^2 \qquad (16)$$

where u_* is the bed shear velocity and u_{*cr} is the critical bed shear velocity = $4w_s/D_*$.

Van Rijn (1984) proposed that sediment pick-up occurred when bed shear velocity (u_*) exceeded the critical bed shear velocity (u_{*cr}); i.e. sediment pick-up is equal to zero when $u_{*cr} > u_*$. This was based on the assumption that the turbulence that drives the sediment pickup rate is entirely generated locally by bed-friction (vdZ et al., 2017b).

The transport parameter of van Rijn (1984) was reformulated to include external breaking generated TKE, making the near-bed TKE (k_b) the main driver for the new formulation as follows:

$$T_\Phi = (u_{*kb}^2 - u_{*cr}^2)/u_{*cr}^2 \qquad (17)$$

$$u_{*kb} = c\mu^{1/4}\sqrt{k_b} \qquad (18)$$

where u_{*kb} = adapted bed shear velocity, $c\mu$ = constant = 0.09, k_b = the sum of the locally produced bed shear TKE (k_*) and external breaking generated TKE (k_{wbr}).

When there is no external breaking generated TKE (i.e. $k_{wbr} = 0$), $k_b = k_*$ and sediment entrainment is entirely driven by the locally produced bed shear. Note: the model of vdZ17 was only validated against the SINBAD and CROSSTEX experiments, as the cross-shore (u'), alongshore (v') and vertical (w') fluid velocities were not collected under the SandT-Pro and LIP experiments.

Proposed model – L19

Suspended sediment transport in the surf zone is a function of numerous hydrodynamic and sediment related parameters. In particular, it is important to adequately represent the relationship between sediment entraining forces and settling forces in order to model how much sand is in suspension at any given time. Existing studies covered in this section have incorporated parameters such as the Shields Parameter or bed shear stress and bed shear velocity (e.g. MS92, SR93, SP04, VR07), fluid velocities (e.g. JS07) and near-bed turbulent kinetic energy (e.g. vdZ17) to represent the entraining forces, and parameters such as gravitational acceleration or the settling velocity to represent settling/grounding forces. Herein, a new solution for representing the entraining forces is proposed. When tested against monochromatic, regular (e.g. *SandT-Pro* and *SINBAD* datasets) and irregular waves (*CROSSTEX* and *LIP* datasets) C_0 in the nearshore region (between the shoaling and breaking zones) was found to have a strong inverse relationship with the local water depth, up until the wave plunging point.

$$C_0 \propto 1/d \qquad (19)$$

I.e. as the cross-shore measurements went from the shoaling zone to the breaker zone, local water depth decreased in the onshore direction, and corresponding measured SSC increased (see Fig.12). In the vicinity of the breaking point (generally at the bar crest) and the plunging point (generally at the bar trough) where water depths were lowest, the measured SSC was found to be highest. The (relative) water depth is also commonly incorporated in reference concentration models– sometimes in combination with the wave height (H/d) – as a measure of the wave breaking intensity and depth penetration of surface generated forces (e.g. Mocke & Smith, 1992). As such, it is proposed that by using the inverse water depth as a key driving parameter, the reference concentration can be modelled empirically. The inverse water depth parameter also takes into the consideration the location of the bar, the development of the bar with time and the breaking/plunging points which can often be determined qualitatively from the bar profile (e.g. breaking often occurs at bar crest) – all of which can influence the suspended sand concentration. The sediment settling forces are incorporated in the proposed formulation via the gravitational acceleration.

Other factors that are considered important to include in sediment pickup and reference concentration models are the wave climate and fluid and sediment characteristics. The wave climate (e.g. wave height, length, period, celerity) is often used in C_0 models as a measure (e.g. size and/or strength) of the forcing wave conditions. The wave height, period, length and celerity are incorporated in the proposed formula – some directly and others as constituent parameters in the roller energy dissipation (D_r) term of Nairn et al. (1990) that was used in the C_0 formulation of Spielmann et al., (2004). The roller energy dissipation (D_r) parameter is important both practically (in terms of its constituent parameters) and conceptually. Practically, the D_r formula incorporates many of the aforementioned parameters that are key drivers of SSC, including the wave climate (wave height, length and celerity) and fluid density. With regards to sediment transport, the incorporation of the breaking roller (roller energy and roller energy dissipation rate) essentially accounts for the effects of rapid wave decay, which occurs in the transition zone between shoaling and inner surf zones, on the reference concentration (c.f. Spielmann et al., 2004).

Fluid characteristics such as the density and viscosity can also have effects on the sediment suspension and settling rates, as can the sediment characteristics such as the sediment density and grain diameter (e.g. generally larger grains are more resistant to entraining forces and settle faster once suspended; smaller grains are more prone to suspension and settle gradually). The sediment characteristics were incorporated via the dimensionless grain diameter (D_*) of van Rijn (2007). Including the grain diameter into reference concentration formulations is of particular importance when attempting to apply the proposed model to different conditions or field locations with multiple sediment fractions – in the present study only single sediment fractions are tested with average grain diameter in the range of D_{50} = 0.22-0.25mm (refer to section 3 of the present study). Based on the above mentioned key driving parameters, the following formula was proposed for reference concentration in kg/m^3 at the reference level of $100D_{50}$:

$$C_0 = (\gamma D_*)^{-0.695} * g(\omega/\mathrm{Dr})^{1.9} * T/d \qquad (20)$$

where
γ = 0.0464 = constant
ω = constant related to cross-shore region

For erosive cases:
ω = 7.5-15.0 for shoaling and breaking regions
ω = 1.0-3.0 for inner surf zone

For accretive cases:
ω = 1.5 for breaking and shoaling zones
ω = 0.6 for inner surf zone

The ω constants empirically account for different (combinations of) suspension mechanisms found in the different cross-shore zones. The values of ω were derived empirically via a 'best-fit' method based on the computed vs. measured reference concentration using the SINBAD and LIP datasets only. Before applying these constants in Eq.20, users must determine whether conditions are erosive – i.e. lead to erosion; which generally consist of relatively larger wave heights combined with shorter wave periods, or accretive – i.e. lead to accretion; which generally consist of relatively smaller wave heights combined with longer wave periods – c.f. section 3.

2.2 Concentration Profile and Mixing Parameter

This section briefly describes the various formulations used to model the concentration profile and mixing parameters throughout this study.

SR93:
Under the assumption that the diffusion coefficient is normally taken to be proportional to the eddy viscosity of flow, and on the basis of experimental data, Okayasu (1989) suggested a relationship with a linear distribution of eddy viscosity (ν_t) as proportionate to the rate of wave energy dissipation due to wave breaking (D_B).

This was estimated by Thornton & Guza (1983) as:

$$D_B/\rho = kH^3g/4Td \qquad (21)$$

where k is a constant related to the breaker type.

The effect of shear due to normal alternating flows under waves was introduced into the diffusion coefficient under breaking waves to produce the following:

$$\varepsilon_b = \{k_1 * u_* + k_2[H^3g/(4Td)]^{1/3}\}\, z \qquad (22)$$

where k_1 and k_2 are constants: k_1 = 0.04 and k_2 = 0.450 for plunging, 0.114 for spilling breakers and 0.216 for transitional breakers.

The commonly used power function can be used to model the concentration profile (e.g. Aagard & Jensen, 2013):

$$C(z) = C_0\,(z_0/z)^M \qquad (23)$$

where M is the mixing parameter

$$M = w_s/\varepsilon_b \qquad (24)$$

For irregular waves, the significant wave height and peak period may be used for the evaluation of parameter M (SR93).

MS92, SP04, JS07, VR07 and vdZ17:

JS07 accounted for local TKE by including the shear velocity under the wave-current co-existent field (u_{*wc}) to the breaking energy dissipation model of Rattanapitikon & Shibayama (1998). Though elements of turbulent velocities induced by both waves (e.g. orbital velocity) and currents (e.g. shear velocity) have been incorporated into the formulation, it seems that the highly turbulent velocities induced by breaking-generated vortices are not adequately accounted for.

The concentration profile and mixing parameter were computed using Eqs.23 & 24, but a different diffusion coefficient was used as follows:

$$\varepsilon_b = k_1 * u_{*wc} + k_2 * (D_B/\rho)^{1/3} \qquad (25)$$

where k_1 and k_2 are constants: $k_1 = 0.08$ and $k_2 = 0.480$ for plunging and 0.225 for spilling breakers.
u_{*wc} = shear velocity under wave-current coexistent field

$$D_B/\rho = 0.15\, c \cdot g/8d\, \{H^2 - [d \cdot exp(-0.36\text{-}1.25\, d/\sqrt{(L \cdot H)})]^2\} \qquad (26)$$

D_B = average rate of wave energy dissipation due to wave breaking computed from the empirical relationships in Rattanapitikon & Shibayama (1998).

L19:

Again, Eq. 23 was used to compute the concentration profile, but a different mixing parameter was implemented. The standard mixing parameter exponent used in the Rouse profile is derived as a function of the settling velocity and bed shear velocity as follows:

$$M = w_s/\kappa u_* \qquad (27a)$$

where κ is the von Karman constant (=0.4). This mixing parameter was empirically modified based on simple sensitivity analysis and best fit techniques when compared against measured data as follows:

$$M = w_s/1.64 u_* \qquad (27b)$$

3. Overview of Experimental Datasets

In this section a brief description is given regarding the various experimental datasets used in this report for validation purposes. This section will cover the facility in which the data was collected, test conditions and profile evolution. As only a general description of the data is presented in this section, readers are directed to the original works for more detailed descriptions of the datasets and experimental conditions. Note: the coordinate system in this report indicates x positive onshore and z positive upward from the bed – i.e. x=0 is at wave paddle and z=0 is at the bed.

LIP Experiments – Roelvink & Reniers (1995)
Only test cases 1b and 1c of the LIP experiments were used in this report:

Table 1 – Summary of experimental conditions for the *LIP* Experiments

Flume	Delta Flume at Delft Hydraulics: L225m x W5m x D7m
Breaker bar	Yes. Erosive case: offshore bar migration, accretive case: onshore bar migration
Mobile sand bed	Yes: D_{50} = 0.22mm
Measured settling velocity	Erosive case: 0.03m/s, accretive case: 0.028m/s
Regular or Irregular waves	Irregular (erosive and accretive)
Breaker types	Spilling and plunging
Offshore wave height (H_0)	erosive case: 1.4m, accretive case: 0.6m
Offshore wave period (T)	erosive case: 5s, accretive case: 8s
Duration of runs and number of repeats	erosive case: 18x1hr runs, accretive case: 13x1hr runs
Number of cases used in present study	9 erosive cases + 7 accretive cases = 16 cases

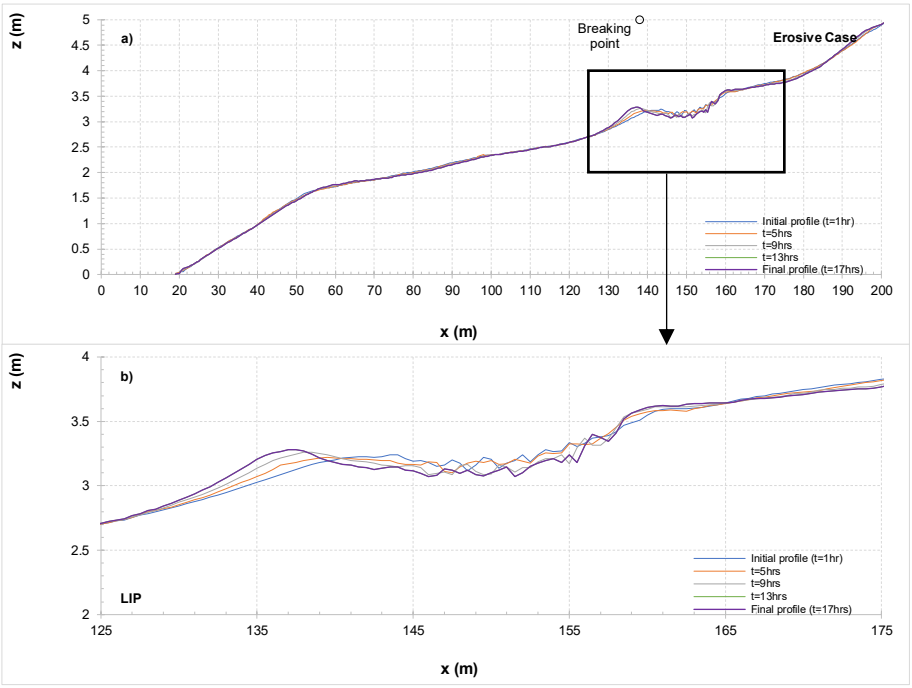

Figure 1 – Cross-shore profile evolution of *LIP* Experiments (Erosive case) – a) shows the whole cross-shore profile, and b) zooms in on the breaker region.

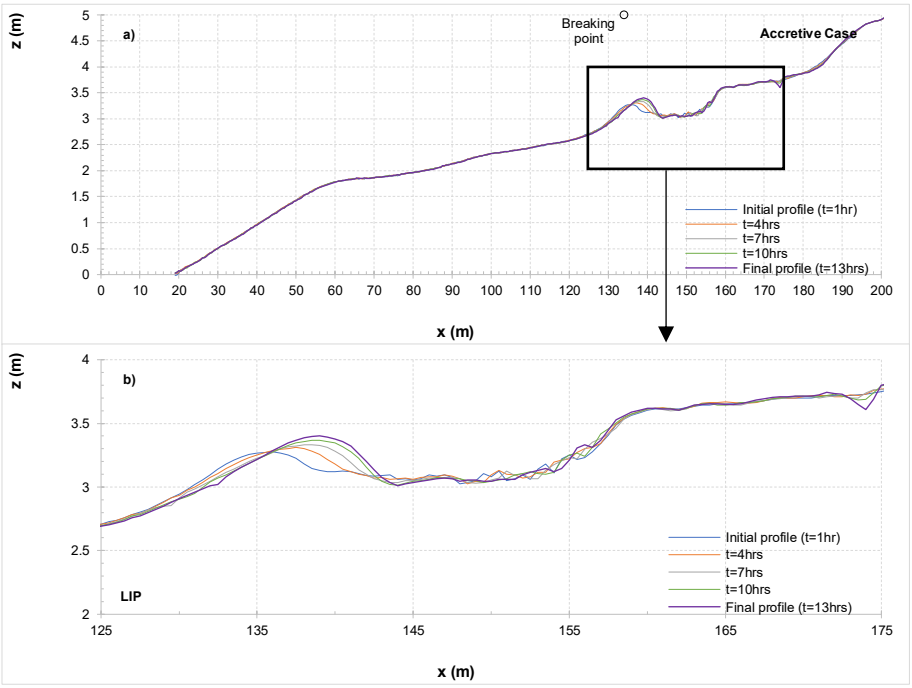

Figure 2 – Cross-shore profile evolution of *LIP* Experiments (Accretive case) – a) shows the whole cross-shore profile, and b) zooms in on the breaker region.

The initial profile was flat in test 1a. As the tests progressed, the final profile of 1a was used as the initial profile of test 1b, the final profile of test 1b as the initial profile of 1c and so on until the final test was completed. Tests 1a-c and 2a-e were run. The measurements used in this study were carried out under two types of irregular waves, leading to different morphological development in each of the observed cases. Test 1b (Fig.1) was carried out in erosive conditions. Figure 1a shows that the breaker bar develops throughout the duration of the runs, with the bar crest increasing in height and migrating in the offshore direction. Test 1c (Fig.2) was carried out in the accretive conditions. With strong plunging breakers predominant in this case, bar development is seen to be more significant. Bar migration occurs in the onshore direction. Though it is difficult to set one particular cross-shore location as the breaking or plunging point under irregular wave conditions, estimations were made for the purpose of comparison between measured and computed concentration. Based on hydrodynamics, profile evolution and

corresponding sediment concentration measurements the breaking point was estimated to be at x=134m and plunging point at x=138m.

CROSSTEX Experiments – Yoon & Cox (2010)

Table 2 – Summary of experimental conditions for the *CROSSTEX* Experiments

Flume	O H Hindsdale Laboratory, Oregon State University – L104m x W3.7m x D4.6m
Breaker bar	Yes: Erosive case – offshore bar migration, accretive case – onshore bar migration
Mobile sand bed	Yes: D_{50} = 0.22mm
Measured settling velocity	N/A – computed settling velocity ≈ 0.032m/s
Regular or Irregular waves	Irregular (erosive and accretive)
Breaker types	Spilling and plunging
Offshore wave height (H_0)	erosive case: 0.6m, accretive case: 0.4m
Offshore wave period (T)	erosive case: 4s, accretive case: 7s
Duration of runs and number of repeats	15-45min runs, erosive case: total 180mins, accretive case: total 300mins
Number of cases used in present study	11 erosive cases + 9 accretive cases = 20 cases

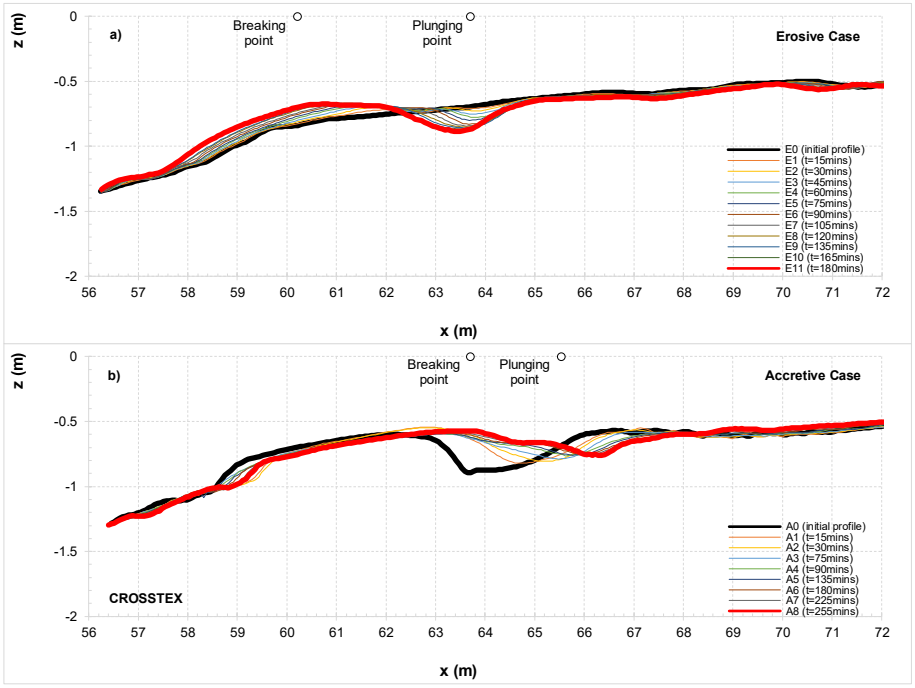

Figure 3 – Cross-shore profile evolution of *CROSSTEX* Experiments

As observed in the LIP experiments, here also two different test conditions were used, resulting in different morphological changes. The bed profile in the erosive case was initially planar. The formation of a sand bar can be observed in Fig.3a, with offshore bar migration in the erosive case. The accretive case saw the barred bed being restored to a planar bed, with onshore migration of the bar. Again, the breaking/plunging points were not explicitly stated, but the breaking point was estimated to be at x=61m and the plunging point (for waves that plunged) was estimated to be at x=63.7m for the erosive cases. For the accretive cases, the breaking point was at x=63.7m and the plunging point was at x=65.5m. It should be noted that in the erosive case, breakers were predominantly spilling and in the accretive, predominantly plunging. For simplicity however, the point at which the wave spills or plunges in erosive cases will also be referred to as the plunging point throughout this study.

SandT-Pro Experiments – Ribberink et al. (2014)

Only test case RB1 of the SandT-Pro experiments was used in this report:

Table 3 – Summary of experimental conditions for *SandT-Pro* Experiments

Flume	CIEM Flume at Polytechnic University of Catalunya, Barcelona: L100m x W3m x D4.5m
Breaker bar	Yes – onshore bar migration
Mobile sand bed	Yes: D_{50} = 0.246mm
Measured settling velocity	0.034m/s
Regular or Irregular waves	Regular monochromatic
Breaker types	Plunging
Offshore wave height (H_0)	0.85m
Offshore wave period (T)	4s
Water depth at wave paddle	2.55m
Duration of runs and number of repeats	13runs x 15-30mins = total run time of 365mins
Number of cases used in present study	Only RB1 test used = 11 cases

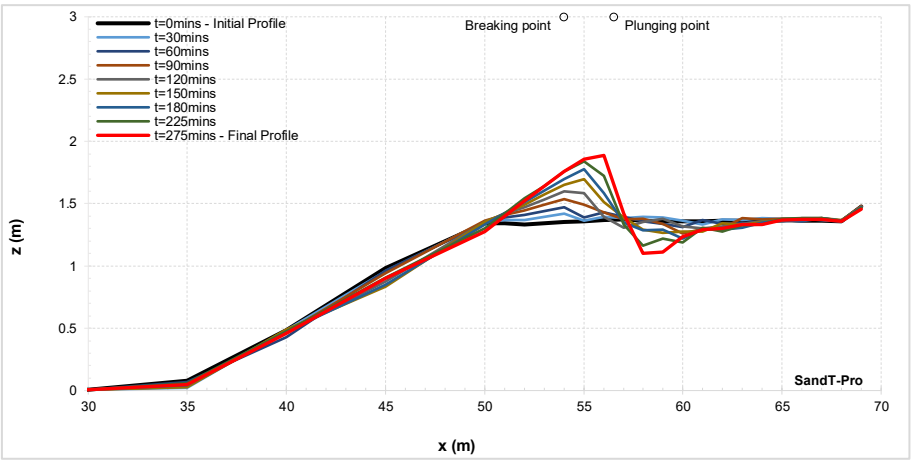

Figure 4 – Cross-shore profile evolution of *SandT-Pro* Experiments

Two different test conditions were carried out in the SandT-Pro experiments, but only the test case RB1 (regular breaking 1) was used in this study. Wave breaking initiated at x=54m, reported to be approximately 2m before the bar crest (Ribberink et al., 2014). The breaking waves plunged at x=57m (plunging point) just after the bar crest. The bed profile evolved from planar to a barred profile, with some onshore bar migration. After 365mins the bar had fully developed, with a length of approximately 7m and height 60cm, and trough length of approximately 5m with maximum depth of 25cm (Ribberink et al., 2014).

SINBAD Experiments – van der Zanden et al. (2016)

Table 4 – Summary of experimental conditions for *SINBAD* Experiments

Flume	CIEM Flume at Polytechnic University of Catalunya, Barcelona: L100m x W3m x D4.5m
Breaker bar	Yes – onshore bar migration
Mobile sand bed	Yes: D_{50} = 0.246mm
Measured settling velocity	0.034m/s
Regular or Irregular waves	Regular monochromatic
Breaker types	Plunging
Offshore wave height (H_0)	0.85m
Offshore wave period (T)	4s
Water depth at wave paddle	2.55m

Duration of runs and number of repeats	(6 runs x 15mins) x 12 repeats
Number of cases used in present study	72 cases

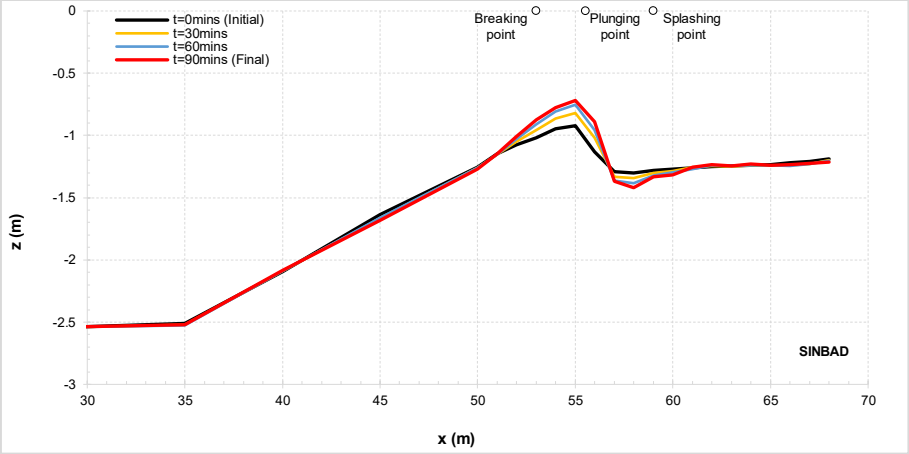

Figure 5 – Cross-shore profile evolution of *SINBAD* Experiments

The wave conditions were the same as those used in the SandT-Pro experiments. The initial profile was however barred in the SINBAD experiments. The breaking initiation occurred at x=53m (breaking point) and plunged at x=55.5m. The splash point was also identified to be at x=58.5m, the point at which the water is pushed up from the plunge and transforms into a surf bore. Based on these cross-shore points, the shoaling region was defined to be x<53m, the breaking region 53<x<58.5m and the inner surf zone x>58.5.

4. Validation of Models

4.1 Reference Concentration and Vertical Mixing

It was found that the coefficient of determination (R^2) is strongly affected by the sample size (i.e. the size of the dataset). In the present study, as can be found in section 3 of this report, the number of measured cases varies greatly between each dataset, with the SINBAD experiments having as many as 72 cases, and the SandT-Pro with only 11 cases used. Sample sizes too large produce very high values of R^2 as the coefficient of determination never decreases, but only increases with added data points. On the contrary, sample sizes too small would also lead to unreliable (very small) values. It is for this reason the root-mean-square error (RMSE) has been used instead to quantitatively compare the performance of the different models. These RMSE values have not been normalised, and therefore are not intended for inter-comparison between datasets, but to compare the performance of the various models against the measured data, and against each other. These RMSE values are summarised in Table 5.

Mocke & Smith (1992) – MS92

LIP: Figure 6a shows that agreement between measured and computed C_0 is generally reasonable for the erosive case. Figure 7a indicates agreement is good in the shoaling (approx. x=115-130m for erosive case) and breaking zones (approx. x=135-165m for erosive case). Even at and around the plunging point (x=138m), where MS92 is seen to under-predict C_0 significantly in other plots (e.g. see Figs.7e-f), it shows good agreement with the measured data. The magnitude of measured concentration at the spilling/plunging point in Fig.7a is consistent with that seen in Fig.7c (approx. 4-5 kg/m^3), which was also measured under erosive irregular wave conditions (predominantly spilling breakers). It is speculated that the difference in observed performance (between Figs.a, c and Figs e-f) is due to the lower levels of breaking-generated TKE found under spilling breakers as the erosive cases consisted predominantly of spilling breakers. This suggests that the model of MS92 is reasonably adept in modelling reference concentration for non-breaking or spilling wave conditions, where there are lower levels of breaking-induced TKE.

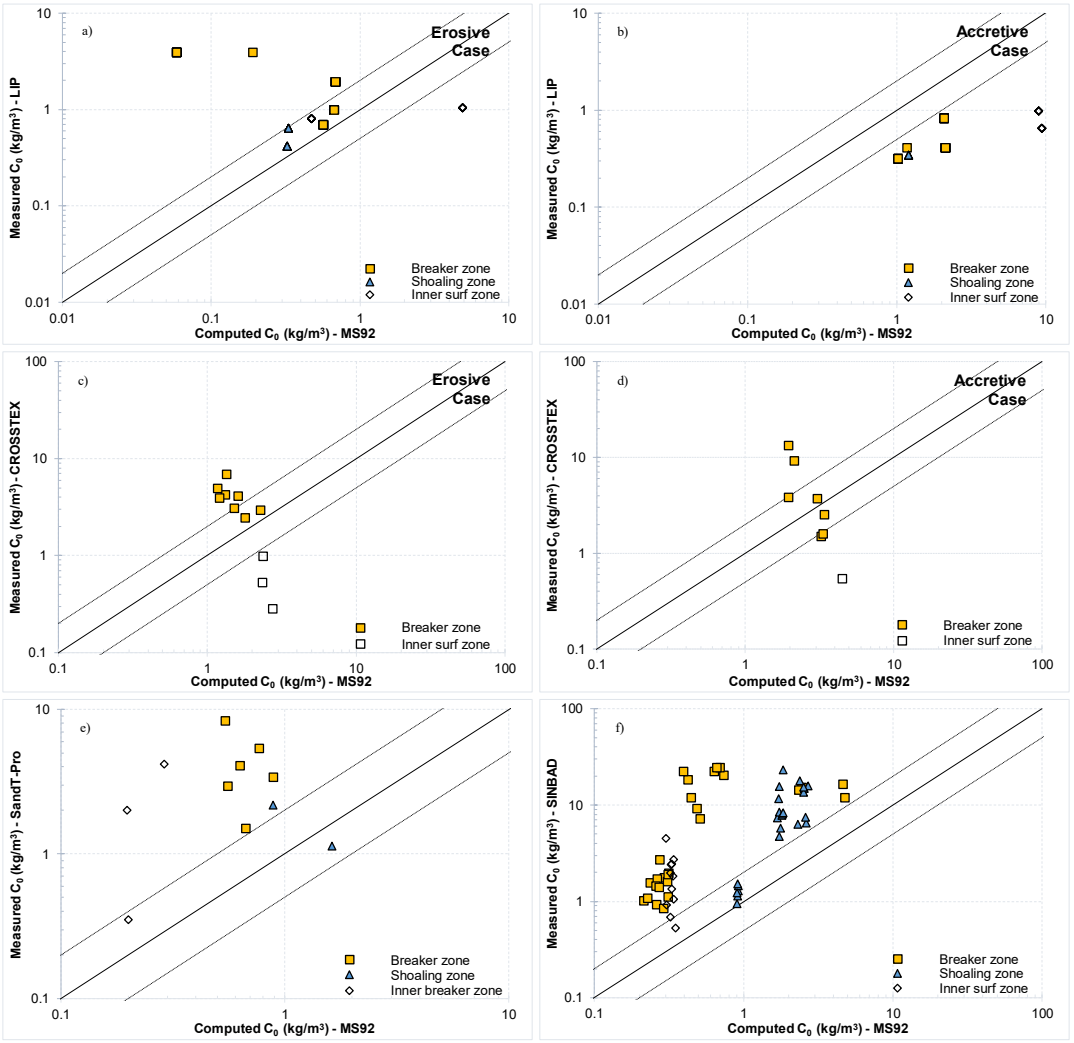

Figure 6 – Measured vs. Computed reference concentration: derived using the model of MS92. Plot a-b) show the MS92 model validated against LIP erosive and accretive conditions respectively; c-d) show validation against CROSSTEX erosive and accretive conditions respectively; e-f) show validation against the SandT-Pro and SINBAD experiments respectively. The solid line indicates perfect agreement between measured and computed, dotted lines indicate computed values being a factor of 2 larger/smaller than the measured – this is referred to throughout this paper as the "factor 2 region".

In the accretive case (Fig.7b), despite breakers being predominantly plunging, the cross-shore variability of measured C_0 is almost linear with steady low levels (<1kg/m^3) of SSC throughout all regions, even at the plunging point (approx. x=134m). This trend is not consistent with the accretive case from the CROSSTEX experiments (Fig.7d) where there are strong localised increases in measured C_0 at the plunging point (x=65.5-67.5m). It is speculated that this inconsistency may be a result of some waves propagating over the breaker bar without breaking (further elaborated in section 5.3), inferring that the constant low levels of measured SSC observed in Fig.7b are a result of bed shear or sediment remaining in suspension due to residual turbulence. Regardless, Fig.7b shows that the low levels of C_0 in the shoaling zone (approx. x=115-132m for accretive case) and breaking zone (approx. x=132-165m for accretive case) are captured reasonably well. Though Fig.6b indicates that all of the points lie outside of the factor 2 region, the discrepancies are generally quite small (in the order of 10^0 kg/m^3) in the shoaling and breaking zones.

CROSSTEX: Contrary to the performance against the LIP datasets, Figs. 7c-d show MS92 under-predicting in the breaking zone, in both the erosive (x=61-64m) and accretive (x=63.7-67.5m) cases. The level of discrepancy between measured and computed C_0 is not as high in the erosive case as the accretive case, with peak concentration levels considerably lower in the erosive cases (≈5 kg/m^3) than in the accretive cases (peak at ≈9.3 kg/m^3, shoreward of the plunging point). The difference in peak concentration is attributed to the predominant breaker types observed in different cases – although both plunging and spilling breakers were present in both test conditions, it was reported that spilling breakers were prevalent in the erosive and plunging breakers in the accretive cases. It is well established in literature that spilling breakers are less effective in entraining

and mixing sediment (e.g. vdZ et al. 2017a) with TKE being spread more gradually upon breaking, in comparison to the rapid spreading of TKE induced by plunging breakers.

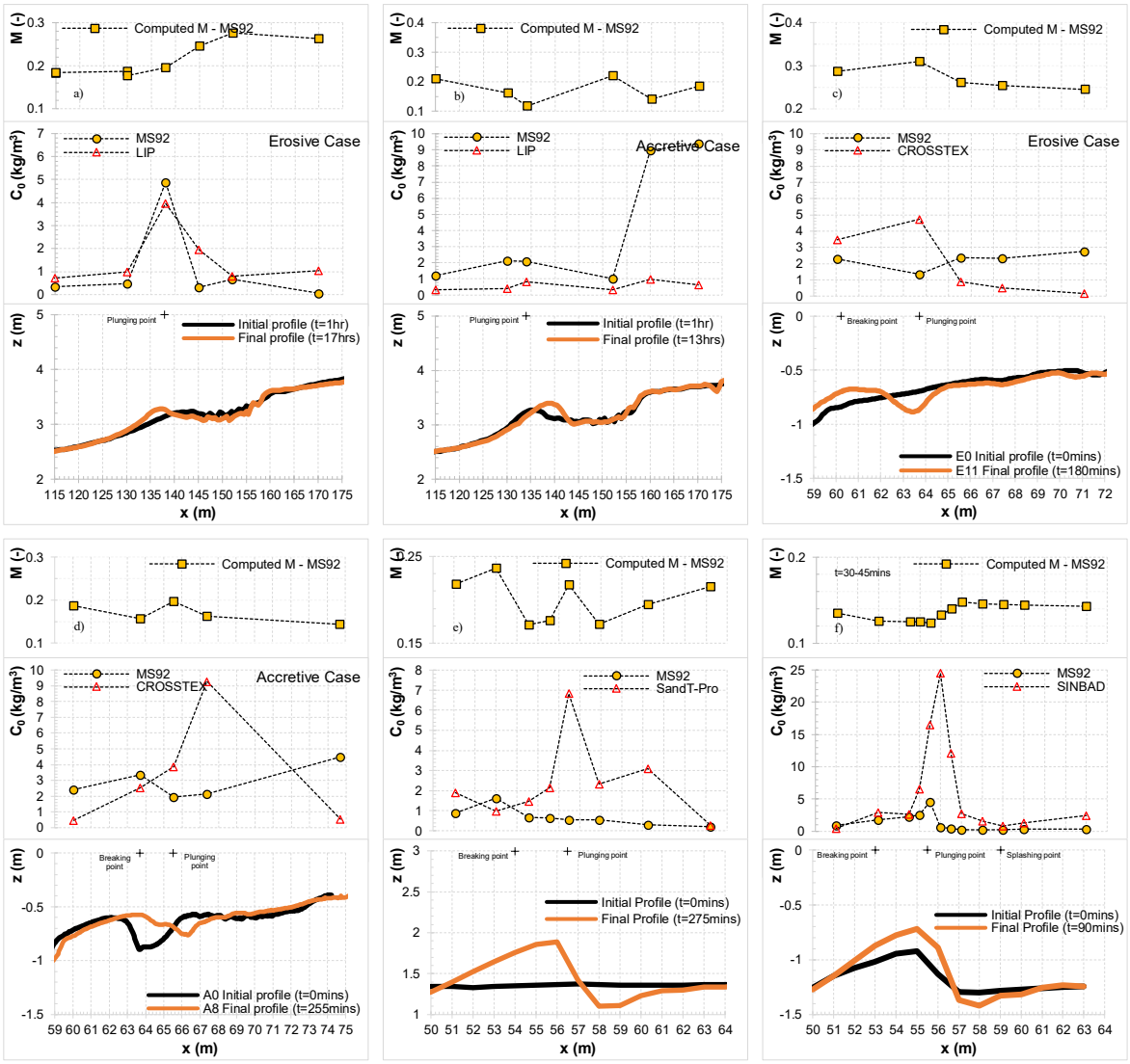

Figure 7 – Cross-shore distributions of mixing parameter (top panels), measured and computed reference concentration (middle panels) and bed profile evolution (lower panels). Plots a-f) show the MS92 model validated against each of the datasets LIP erosive and accretive cases, CROSSTEX erosive and accretive cases, SandT-Pro and SINBAD respectively.

As briefly mentioned above, significant under-predicting is seen around the plunging point (x=65.5-67.5m) in the accretive case (Fig.7d). This is attributed to highly turbulent vortices, induced by wave plunging, invading the WBBL and entraining sediment. It is noted that the measured concentration does not peak at the plunging point, but shoreward of the plunging point (x=67.37m). This is likely due to the effects of horizontal advection, as well as the large-scale vortices continuing to travel obliquely downwards and in the direction of wave propagation as described in section 1. This observation is consistent with that seen in Fig.7f.

SandT-Pro: Though a couple of the points in Fig.6e are within the factor of 2 region, the majority indicate considerable under-prediction of C_0. A quasi-linear computed C_0 variability is observed (Fig.7e) over the various cross-shore zones with the model of MS92, with considerable under-predicting at almost every cross-shore location. This is especially the case at the plunging point (x=56.5m) where the discrepancy between measured and computed C_0 is the largest – just over a factor of 12. This is consistent with observations from other datasets, indicating that the strong localised increase in measured C_0 observed at the plunging point is not adequately accounted for by the model of MS92. The level of discrepancy observed at the shoaling (x=51-53m) and inner surf zones (x=60-63m) is reasonable, indicating good agreement in these zones.

SINBAD: The 30-45mins test cases (of a total run time of 90mins) were considered in the SINBAD case. This is because there

were many instances of data being removed as outliers in other test cases, especially in the highly aerated breaking region (vdZ et al. 2016). The 30-45mins test case did not have missing data in any of the measured regions. Also, it is between 1/3 to 1/2 way through the experiment runs, where the bottom profile and breaker bar have developed quite substantially.

The trends seen in Figs.6f&7f are generally similar to Figs.6e&7e, mainly with respects to the large under-predicting in the breaking zone (x=54.5-59m). Although the computed cross-shore variability of C_0 indicates some localised increase in concentration around the plunging point (x=55.5m), it does not sufficiently reflect the high levels of SSC measured at this point. The computed C_0 at the plunging point was ≈4.6 kg/m^3, whereas the measured C_0 is almost four times greater (≈16.5 kg/m^3).

Mixing parameter: The same mixing parameter was used for MS92, SP04, JS07, VR07 and vdZ17. The cross-shore distributions of the mixing parameter M can be seen in the top panels of Figs.7a-f. The mixing parameter generally captured the localised increases in concentration found at the breaking and plunging points in all cases (M increases at these points). Particularly in Figs.7a&7f, the mixing parameter indicates increases in sediment mixing just shoreward of the plunging point. As mentioned in section 1 of this paper, the combination of trapped bubbles and breaking-generated vortices (generated at the plunging point) enhance sediment mixing throughout the water column. The mixing effects of these turbulent vortices would not be limited to only the plunging point, but also to neighbouring zones as the breaking-induced TKE is advected horizontally. Fernandez-Mora et al. (2016) reported that high in the water column, breaking-generated TKE is partly advected in the offshore direction by undertow and orbital velocities, and party advected in the shoreward direction by onshore velocities under a secondary wave; the remainder of the broken wave (vdZ et al. 2016).

Summary: The level of accuracy varies quite largely between each dataset and also each cross-shore region. The model of MS92 generally performs quite well in the shoaling region, and even in the breaking region, pre-plunging point, for regular waves and irregular erosive wave conditions. Post-plunging however, the MS92 model is not able to capture the strong localised increase in C_0 observed at the plunging point and immediately shoreward of the plunging point. In the accretive conditions, the model shows mixed results, showing poor agreement with the CROSSTEX dataset but reasonable agreement with the LIP dataset. Overall, the model of MS92 does not seem well suited for the breaker (inner-surf zone) where under-(over-)prediction is often observed (see Figs.7b-d), and though it may perform reasonably well for spilling waves (e.g. erosive case), it is not adept for plunging breaker conditions.

Shibayama & Rattanapitikon (1993) – SR93

LIP: SR93 generally shows poor agreement with measured data, with Figs.8c-f showing considerable under-predicting in all cross-shore zones – both erosive and accretive, regular and irregular waves (note: 1 point is not shown in Fig. 8a and 1 point not shown in 8b as the discrepancies between measured and computed were too large to fit in the plot range). However, contrary to the trend observed against other datasets, Figs.8a-b indicate some over-predicting, particularly in the shoaling and inner surf zones (Fig.9a-b). In the accretive case, over-predicting occurs even at the plunging point (x=134m), where the cross-shore variability of measured C_0 is constantly low (<1 kg/m^3) (as seen in Fig.7b).

CROSSTEX & SandT-Pro & SINBAD: almost all of the breaker zone points lie outside of the factor 2 region of Figs.8c-f. Even in the erosive case of CROSSTEX (Fig.9c) where breakers were a mixture of spilling and plunging waves, the model of SR93 is not able to account for the local increase in C_0 at the spilling/plunging point (x=61-64m). This is observed to a greater extent in the accretive case, with larger discrepancies found at the plunging point (x=65.5-67.5m). Figures 9e-f indicate that the cross-shore variability of computed C_0 are very similar to that observed in Fig.7e; they are quasi-linear with largest discrepancies in the breaker zone (between x=55.5-59m for SandT-Pro, and x=54.5-57m for SINBAD) and also early in the inner surf zone (around x=60m for SandT-Pro). As seen with the MS92 model, discrepancies are especially large at the plunging point, where there are sharp increases in measured concentration. This localised increase in C_0 at the plunging point is not captured by the SR93 model, with computed C_0 being smaller than measured (Fig.9e) by a factor of 14. The same is observed against the SINBAD experiments, with even larger discrepancies (see Fig.9f). This is not surprising as the SR93 formulation is driven mainly by the shear velocity and relies on the Shields Parameter to predict sediment pickup. vdZ et al. (2017a) reported that time-averaged reference concentrations showed poor correlation with periodic and time-averaged near-bed velocities, but significant correlation with near-bed time-averaged TKE. As such, the constant under-predicting of computed C_0 in the breaker zone suggests that the model is not adept for strong plunging conditions and needs to more effectively incorporate near-bed TKE to improve the formulation.

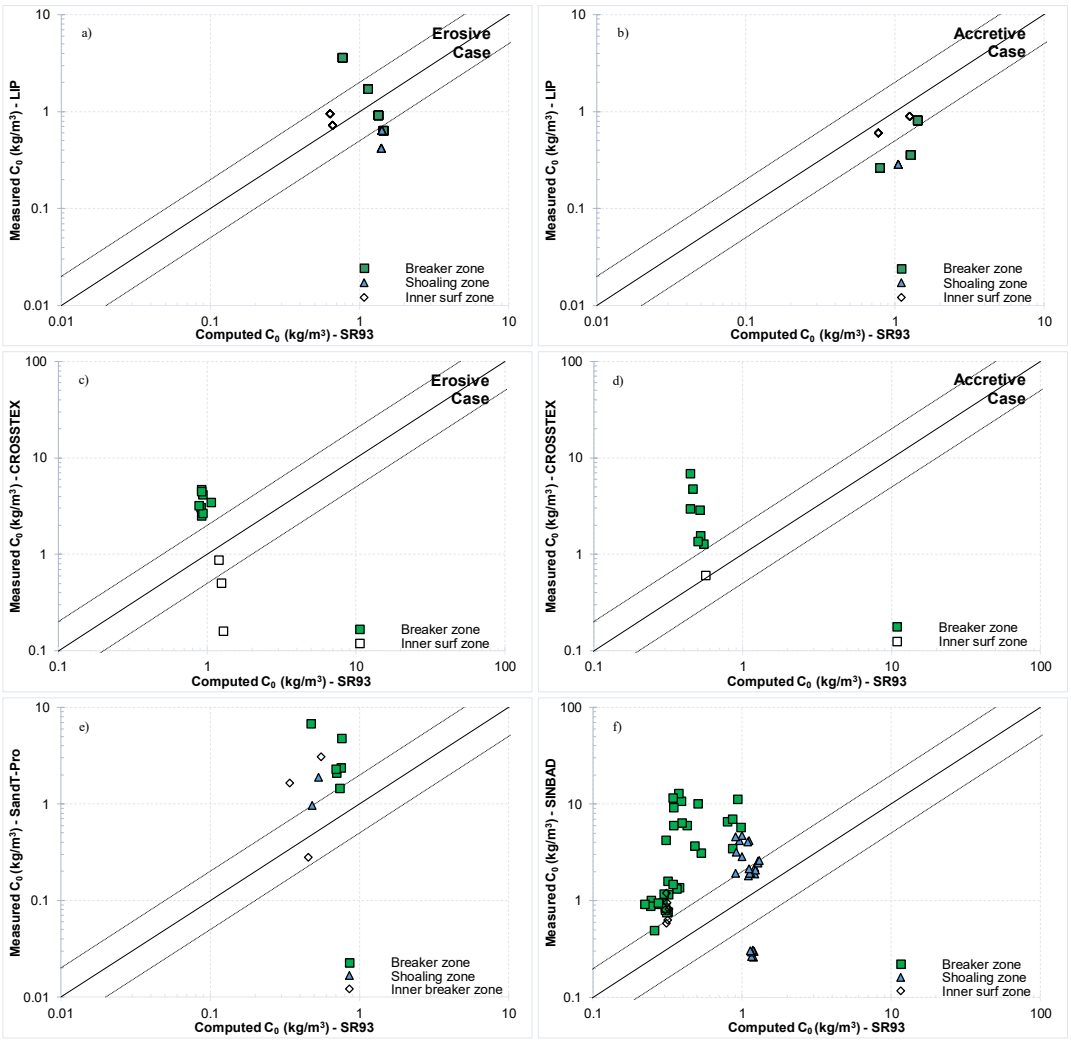

Figure 8 – Measured vs. Computed reference concentration – derived using the model of SR93. Plot a-b) show the SR93 model validated against LIP erosive and accretive conditions respectively; c-d) show validation against CROSSTEX erosive and accretive conditions respectively; e-f) show validation against the SandT-Pro and SINBAD experiments respectively.

Summary: The model of SR93 generally performs reasonably in the shoaling and inner surf zones, with computed C_0 in the correct order of magnitude. It performs poorly in the breaker zone however, especially post-plunging. Instead of computed C_0 increasing (relative to the shoaling zone) at the plunging point as indicated by measured SSC, it decreases. This is due to the key driving parameters (e.g. the near-bottom velocity at the breaking point $\hat{u}_b$; Eq.10), which correlates poorly with time-averaged reference concentration, and the Shields Parameter (Eq.3a) formulation which is dependent on the local wave height and water depth. This is discussed further in the validation of the model of SP04 below. Overall, the SR93 model requires modification to account for the entraining and mixing effects of external breaking-induced TKE.

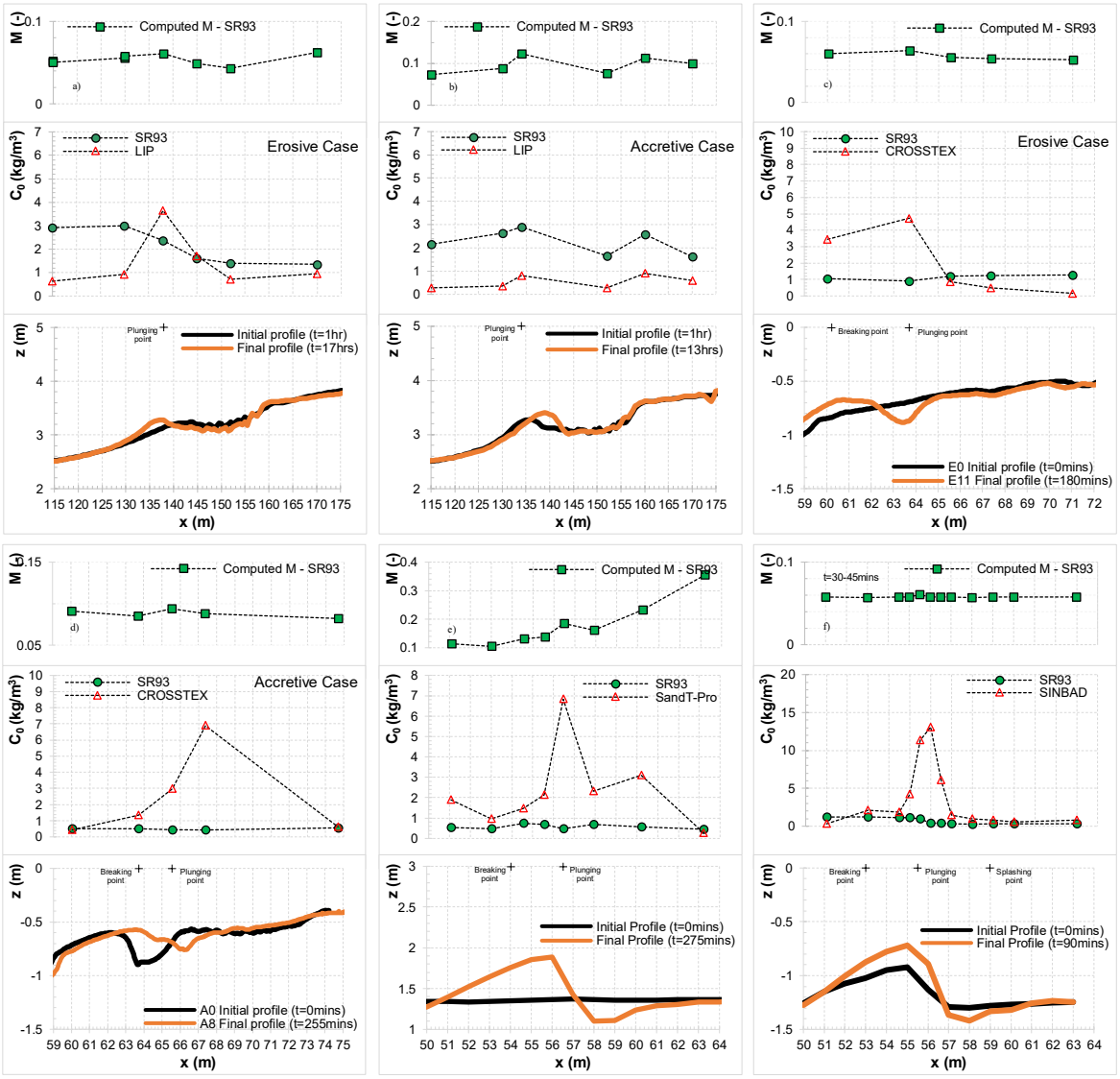

Figure 9 – Cross-shore distributions of mixing parameter (top panels), measured and computed reference concentration (middle panels) and bed profile (lower panels). Plots a-f) show the SR93 model validated against each of the datasets LIP erosive and accretive cases, CROSSTEX erosive and accretive cases, SandT-Pro and SINBAD respectively.

Spielmann et al. (2004) – SP04

SandT-Pro: The model of SP04 shows poor agreement with measured data, with just less than half of the points lying within the factor 2 region in Fig.10e. The computations for the shoaling zone over-predict and those for the inner-surf zone under-predict substantially. Similar to the SR93 and VR07 models, the computed C_0 decreases (relative to the shoaling zone) at the plunging point instead of increasing. This common trend is attributed to the key driving parameters in the SR93, VR07 and SP04 formulations being a function of the local wave height and water depth - which decline steeply at the plunging point. The wave heights (and water depth) are highest in the shoaling region as the waves shoal, and lowest at the plunging point (see Fig.12). This trend is reflected in almost all of the cross-shore variability of C_0 for the SP04 model (see Figs.11a, c-f).

One of the key parameters in the SP04 formulation is the roller energy dissipation term, which is a function of the roller energy term E_r. Different methods/formulae for modelling the roller energy term exist in literature (c.f. Nairn et al., 1990). The empirical method implemented in this study models the roller energy as a function of the local wave height (H) (refer to Eq.9). Considering the relationship between wave height and C_0 shown in Fig.12, this explains the strong over-prediction of C_0 in the shoaling zone, and the gradual decrease in SSC in the shoreward direction throughout the cross-shore regions (i.e. cross-shore distribution of computed C_0 mirrors cross-shore distribution of measured H, with C_0 being largest in shoaling zone, gradually smaller in breaker zone and smallest in the inner surf zone). It should be noted that the performance of the SP04 model could

vary depending on the method/formulation adopted for computation of the roller energy term. It is however beyond the scope of the present study to investigate the effects of different roller energy formulations on resulting reference concentration, and therefore the performance of the SP04 C_0 formula is only tested herein using the empirical method of Svendsen (1984) as specified in section 2.1 (Eq. 9).

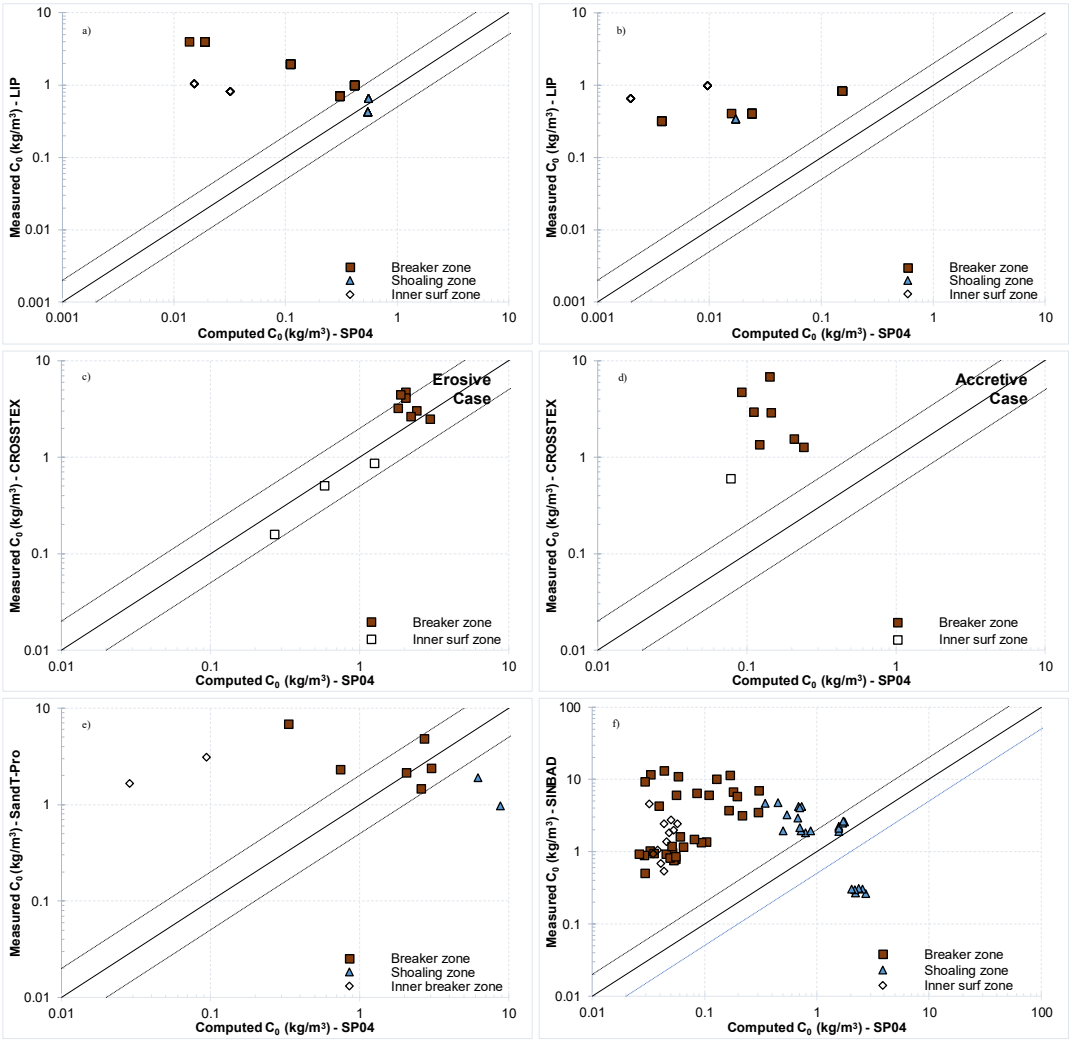

Figure 10 – Measured vs. Computed reference concentration – derived using the model of SP04. Plot a-b) show the SP04 model validated against LIP erosive and accretive conditions respectively; c-d) show validation against CROSSTEX erosive and accretive conditions respectively; e-f) show validation against the SandT-Pro and SINBAD experiments respectively.

LIP & CROSSTEX (Accretive) & SINBAD: The same trend is observed in the LIP, CROSSTEX (accretive) and SINBAD experiments, with the cross-shore C_0 distribution gradually decreasing in the shoreward direction, from the shoaling to inner surf zones. This again is to be expected, as the cross-shore distribution of computed C_0 mirrors the cross-shore wave height variability, as seen in Fig.12. In the LIP (erosive case), CROSSTEX (erosive and accretive cases) and SINBAD case (Figs.11a, 11c-d, and 11f respectively), the discrepancy between measured and computed C_0 is highest at the plunging point and just shoreward of the plunging point. It is evident that SP04 is not able to account for the high levels of sediment entrainment induced by breaking-generated vortices post-plunging.

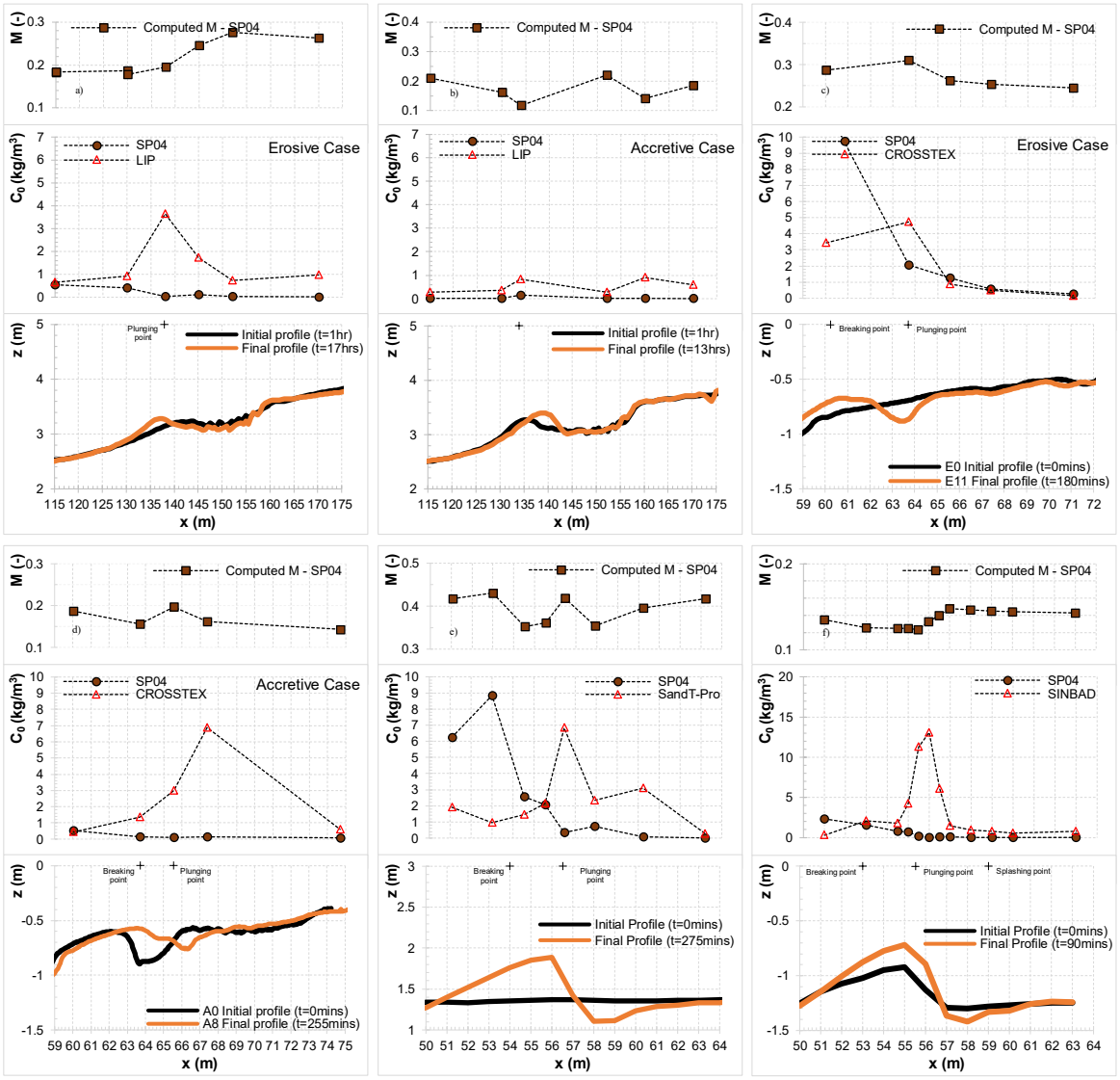

Figure 11 – Cross-shore distributions of mixing parameter (top panels), measured and computed reference concentration (middle panels) and bed profile (lower panels). Plots a-f) show the SP04 model validated against each of the datasets LIP erosive and accretive cases, CROSSTEX erosive and accretive cases, SandT-Pro and SINBAD respectively.

Summary: Similar to the trend observed in the validation of SR93, some of the key driving parameters (e.g. roller energy dissipation term) of the SP04 model are strongly dependent on the local wave height. As a result, the SP04 model is highly sensitive to changes in the local wave height. Local wave height decreases at the plunging point (as seen in Fig.12) and the corresponding computed C_0 also decreases at this point. This leads to large discrepancies between measured and computed C_0, especially at the plunging point. Alternative formulations of modelling the roller area (see Eq.9) may result in improved performance.

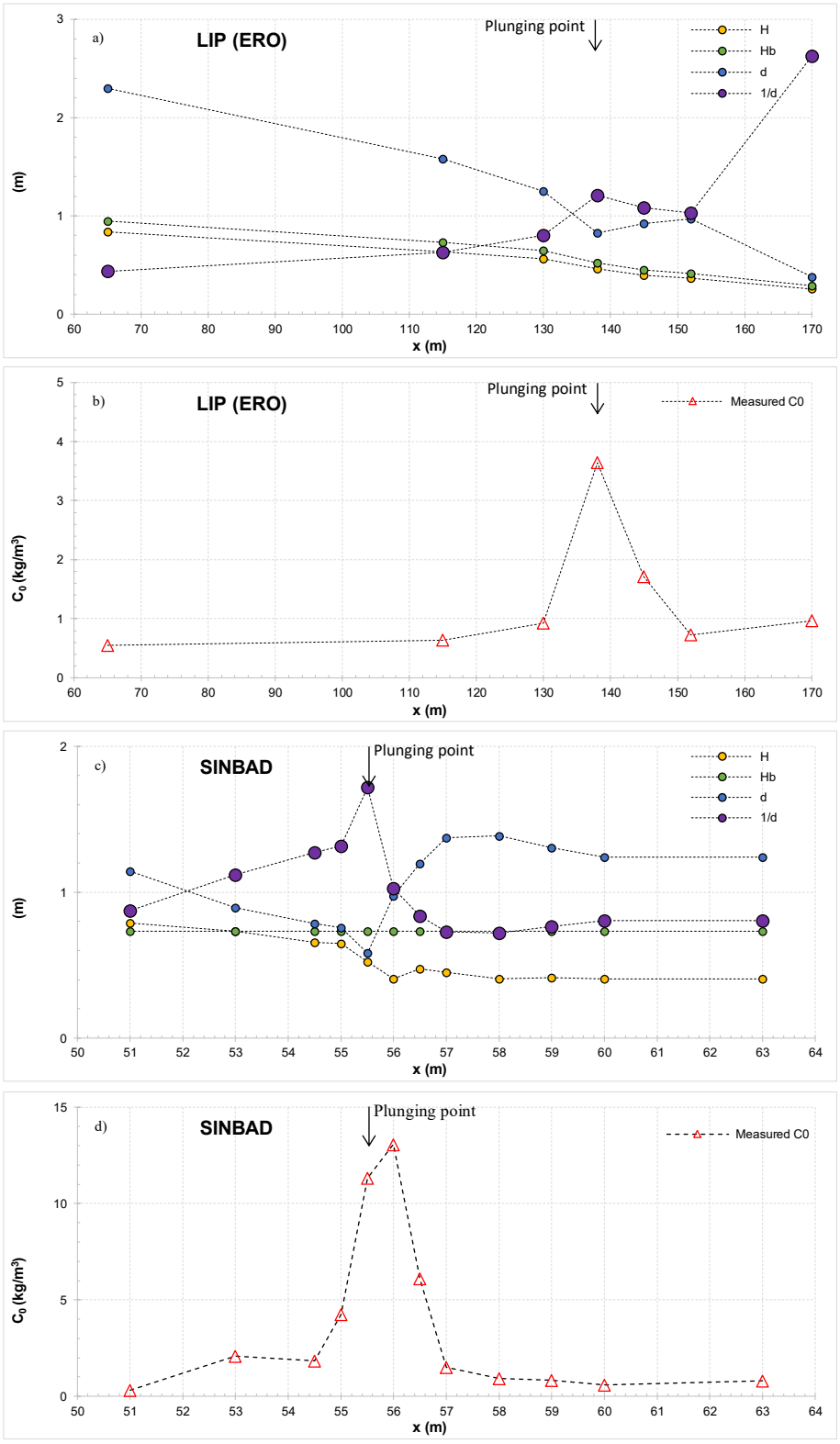

Figure 12 – Cross-shore distributions of local wave height (H), breaker height (H_b), local water depth (d), and inverse water depth ($1/d$) compared against cross-shore distribution of measured reference concentration (C_0). Plots a) and c) show the cross-shore variability of wave climate and (inverse) water depth for LIP erosive case and SINBAD experiments respectively. Plots b) and d) show the cross-shore variability of measured reference concentration for LIP erosive case and SINBAD experiments respectively.

Jayaratne & Shibayama (2007) – JS07

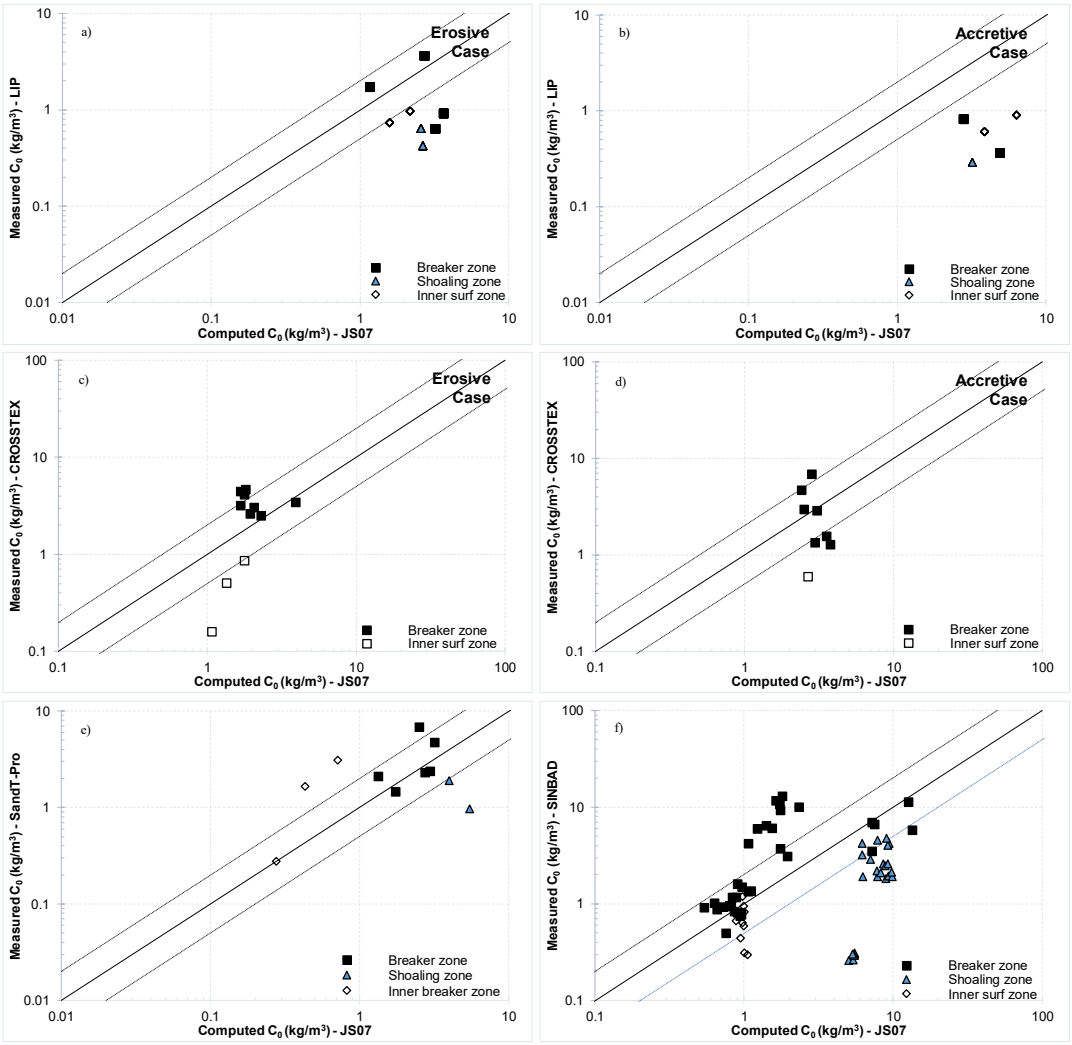

Figure 13 – Measured vs. Computed reference concentration – derived using the model of JS07. Plot a-b show the JS07 model validated against LIP erosive and accretive conditions respectively; c-d show validation against CROSSTEX erosive and accretive conditions respectively; e-f show validation against the SandT-Pro and SINBAD experiments respectively.

LIP: JS07 shows poor agreement with measured data under the erosive case (Fig.13a), with the majority of the points lying outside of the factor 2 region (note: 1 point is not shown in Fig. 13a and 2 points not shown in 13b as the discrepancies between measured and computed were too large to fit in the plot range). It is seen to over-predict C_0 substantially in the shoaling and inner surf zones. There is however some reasonable-good agreement at the breaking point. As mentioned previously in section 2.1, the model of JS07 was only derived and validated for the breaking region, and as such was not designed to predict SSC in the shoaling and inner surf zones.

CROSSTEX: In Fig.13c most of the computed vs measured C_0 values from the breaking zone fall within the factor of 2 margin, indicating good agreement with measured data, even at the plunging point for some test cases (x=63.7m). There is however still discrepancy between measured and computed C_0 near the spilling/plunging point (Fig. 14c-d), both in the erosive (see x=63.7m) and accretive (see x=67.5m) cases. This discrepancy is seen to be larger in the accretive cases where breakers were predominantly plunging waves. Also, in the accretive case, large discrepancies are found in the shoaling region, as seen against the SandT-Pro (Fig.13e) and SINBAD (Fig.13f) datasets.

SandT-Pro: Figure 13e shows reasonable agreement between measured and computed reference concentration, with the points well-clustered around the 1:1 line, over half of points lying within the +/- factor 2 region. Similar to the models of SR93 and SP04, the model of JS07 is driven by parameters (such as near-bed shear velocity, $\hat{u}_b$) that are sensitive to local (or breaker) wave height. As a result, JS07 is generally shown to over-predict concentration in the shoaling zone (see Fig.14a-b and 14d-f), with cases of concentration at the plunging point declining instead of increasing (e.g. Fig.14e) as seen in the validation of

SR93 and SP04. This indicates that the local wave height is a poor driving parameter for cross-shore reference concentration under plunging wave conditions.

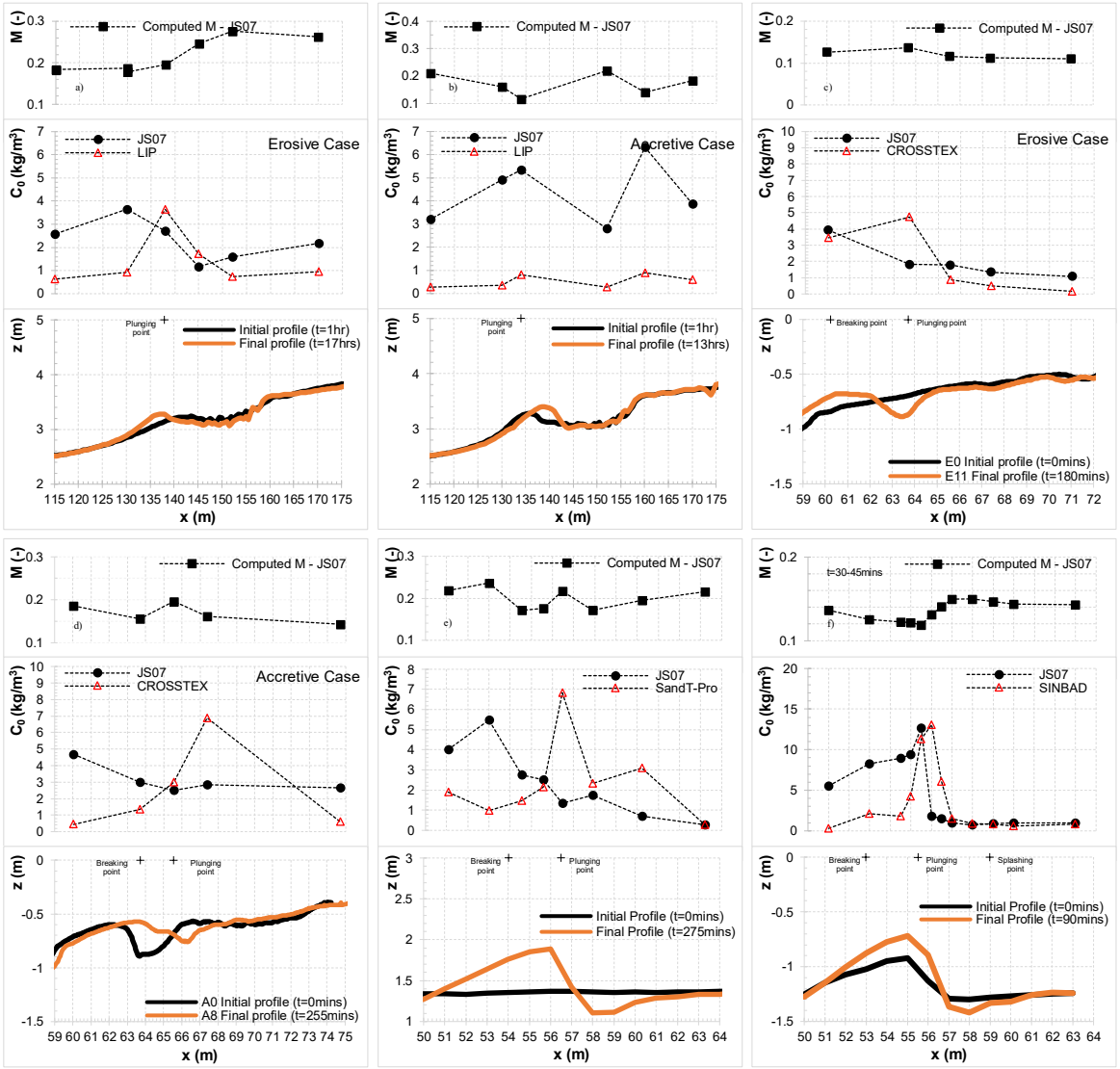

Figure 14 – Cross-shore distributions of mixing parameter (top panels), measured and computed reference concentration (middle panels) and bed profile (lower panels). Plots a-f show the JS07 model validated against each of the datasets LIP erosive and accretive cases, CROSSTEX erosive and accretive cases, SandT-Pro and SINBAD respectively.

SINBAD: The general trend observed in Fig.14f is quite good for the breaker and inner surf zones, but indicates some large over-predicting in the shoaling zone, as seen also against the SandT-Pro data (Fig.14e). Contrary to the trend observed in Fig.14e, the model of JS07 sufficiently captures the strong localised increase in measured C_0 at the plunging point (x=55.5m), indicating very good agreement with measured C_0. However, just after the plunging point (x=56m) where measured C_0 peaks, there is seen to be a large discrepancy as computed C_0 suddenly drops drastically. This can be attributed to the drop in local wave height (H) after the wave plunging point. The agreement between measured and computed C_0 is very good in the outer breaker zone/inner surf zone (between x=57-63m).

Summary: The model of JS07, originally derived only for use in the breaking zone, generally performs well throughout the breaking zone, sometimes even at the plunging point. There are however several instances of the model under-predicting at the plunging point (and just shoreward of the plunging point) where concentration is highest. Similar to the SR93 and SP04 models, the model of JS07 is sensitive to the local wave height, and therefore often over-predicts C_0 in the shoaling zone (where H is highest before breaking, see Fig.12) and under-predicts at the plunging point (where H is lowest after breaking).

Van Rijn (2007) – VR07

SINBAD & CROSSTEX: The model of VR07 shows reasonable cluster around the 1:1 line (Fig.15), with a fair percentage of points being within the factor 2 region. The computed C_0 measurements for the shoaling and inner surf zone are generally quite good, but as commonly seen in the previous models covered in this section, there is major under-predicting especially around the plunging point in all three plots of Fig.16, where breaking-induced TKE invades the WBBL. Very similar to the trend observed with the models of MS92, SR93 and SP04, the local increase in C_0 at the plunging point is not captured by the model (Fig.16) - instead of computed C_0 increasing at the plunging point, it is seen to fall. The validation in this section indicates that reference concentration models driven by bed shear (or Shields Parameter) are not adept for modelling C_0 under plunging breaker conditions, as the effects of surface-generated TKE are not incorporated into the formulations. Such models (e.g. MS92, SR93 and VR07) perform reasonably in non-breaking regions, e.g. shoaling zone. Also, as mentioned in the validation of SR93, vdZ et al. (2017a) reported poor correlations between time-averaged near-bed velocities and time-averaged reference concentration, but good agreement with near-bed TKE. It is thought therefore that VR07 could also be improved by accounting for the high levels of entrainment induced by external breaking-generated TKE, as proposed by vdZ et al. (2017b).

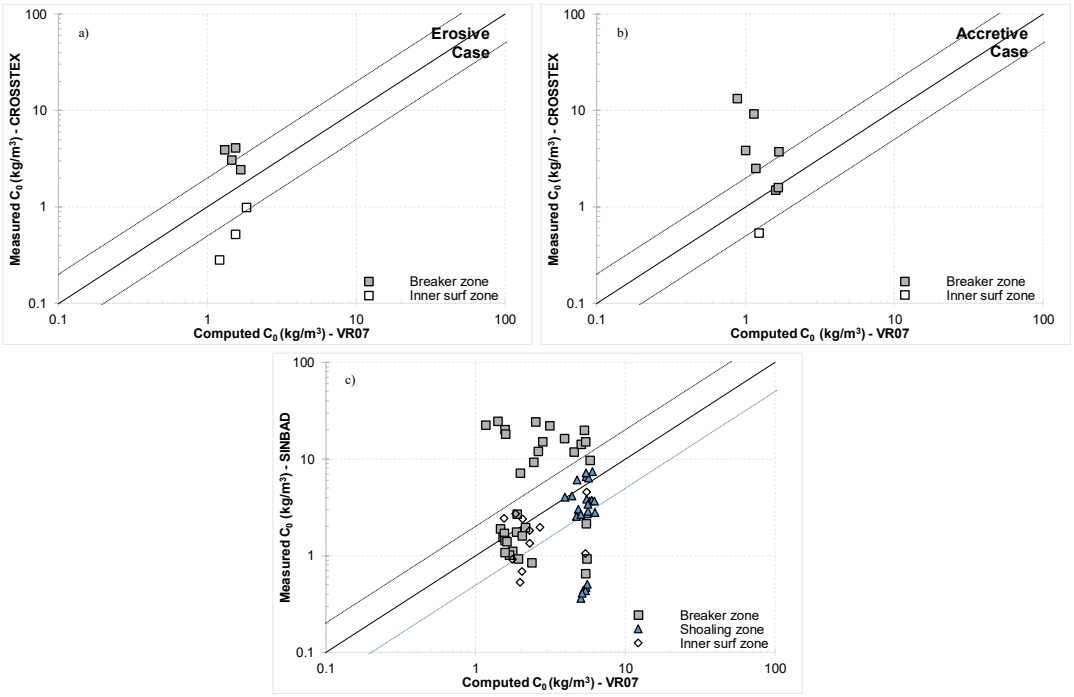

Figure 15 – Measured vs. Computed reference concentration – derived using the model of VR07. Plot a-b) show the VR07 model validated against CROSSTEX erosive and accretive conditions respectively and Plot c) shows validation against the SINBAD experiments.

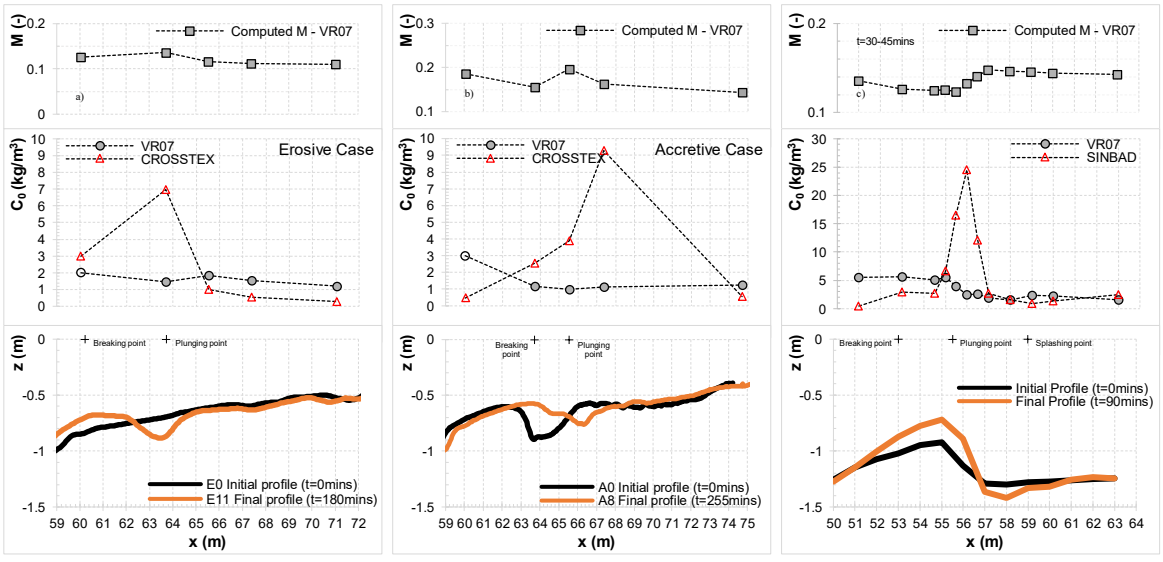

Figure 16 – Cross-shore distributions of mixing parameter (top panels), measured and computed reference concentration (middle panels) and bed profile (lower panels). Plots a-b) show the VR07 model validated against CROSSTEX erosive and accretive cases respectively and Plot c) shows validation against SINBAD cases.

Van der Zanden et al. (2017b) – vdZ17

CROSSTEX: Despite the strong relationship between near-bed TKE and reference concentration reported in literature (e.g. vdZ et al., 2017a; Aagaard et al., 2018), the agreement with measured C_0 in the breaking zone is quite poor in the erosive case. All of the breaker zone points are outside the factor 2 region, indicating mild under-prediction. Almost all of the near-bed TKE (k_b) measurements at 1cm above the bed are missing for the accretive cases, making it difficult to effectively validate vdZ17 model with the CROSSTEX dataset for the accretive case.

SINBAD: Contrary to Figs.17a-b, Fig.17c indicates reasonable-good agreement between vdZ17 and measured data. The model's performance in the breaker zone is quite varied, with some cases of minor over- and under-predicting throughout. Though the strong local increase in C_0 around the plunging point is adeptly captured (with computed C_0 generally in the correct order of magnitude), there is still some under-predicting (in varying extents) at this point.

Comparing the available k_b values between the CROSSTEX and SINBAD datasets has revealed that the values taken at 1cm above the bed at the plunging point differed by approximately a factor of 2. The measured k_b (at 1cm above bed) at the plunging point for the CROSSTEX erosive and accretive cases are very similar in magnitude and are between 0.003-0.006 m^2/s^2. On the other hand, the measurements taken at the same point from the SINBAD experiments are between 0.006-0.01 m^2/s^2. As k_b is one of the main driving parameters for the vdZ17 model, this difference in magnitude in measured k_b has a major effect on the performance of the model, hence the disparity in performance between Figs.18a and 18b. In this section, only the magnitude of k_b has been considered due to the affect it has on the reference concentration formula of vdZ et al. (2017b). Froude-scaled TKE values are compared and discussed in section 5.1 of this report.

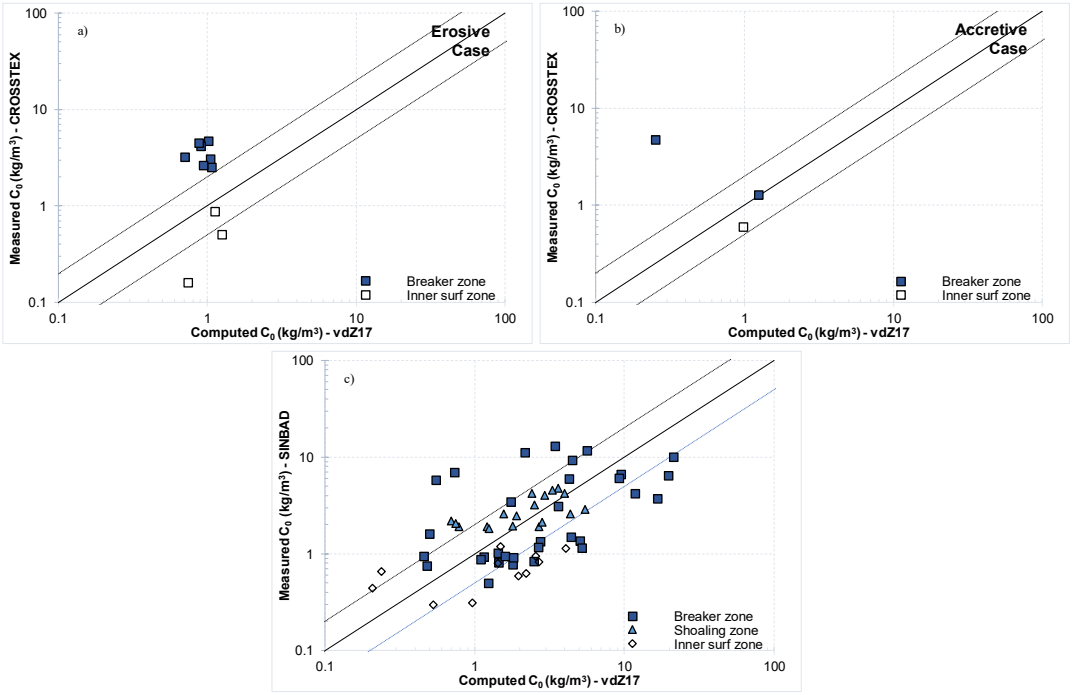

Figure 17 – Measured vs. Computed reference concentration – derived using the model of vdZ17. Plot a-b) show the vdZ17b model validated against CROSSTEX erosive and accretive conditions respectively and Plot c) shows validation against the SINBAD experiments.

Summary: The model of vdZ et al. (2017b) shows varied performance between the different datasets. As k_b is the main driving parameter in the vdZ17 formulation, the magnitude of measured k_b has a large effect on its performance. The significant difference in magnitude of measured k_b between the two datasets will be discussed further in section 5.1.

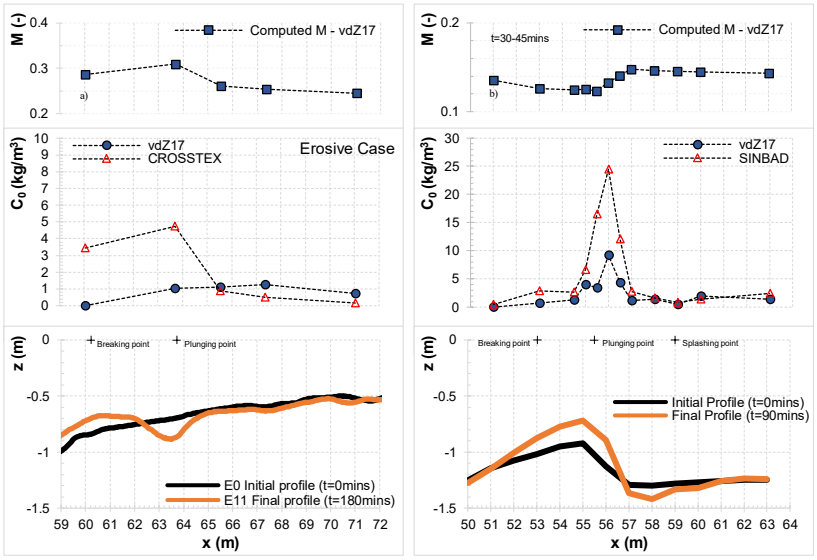

Figure 18 – Cross-shore distributions of mixing parameter (top panels), measured and computed reference concentration (middle panels) and bed profile (lower panels). Plots a-b show the vdZ et al. 2017b model validated against CROSSTEX erosive cases and SINBAD respectively.

Proposed model – L19

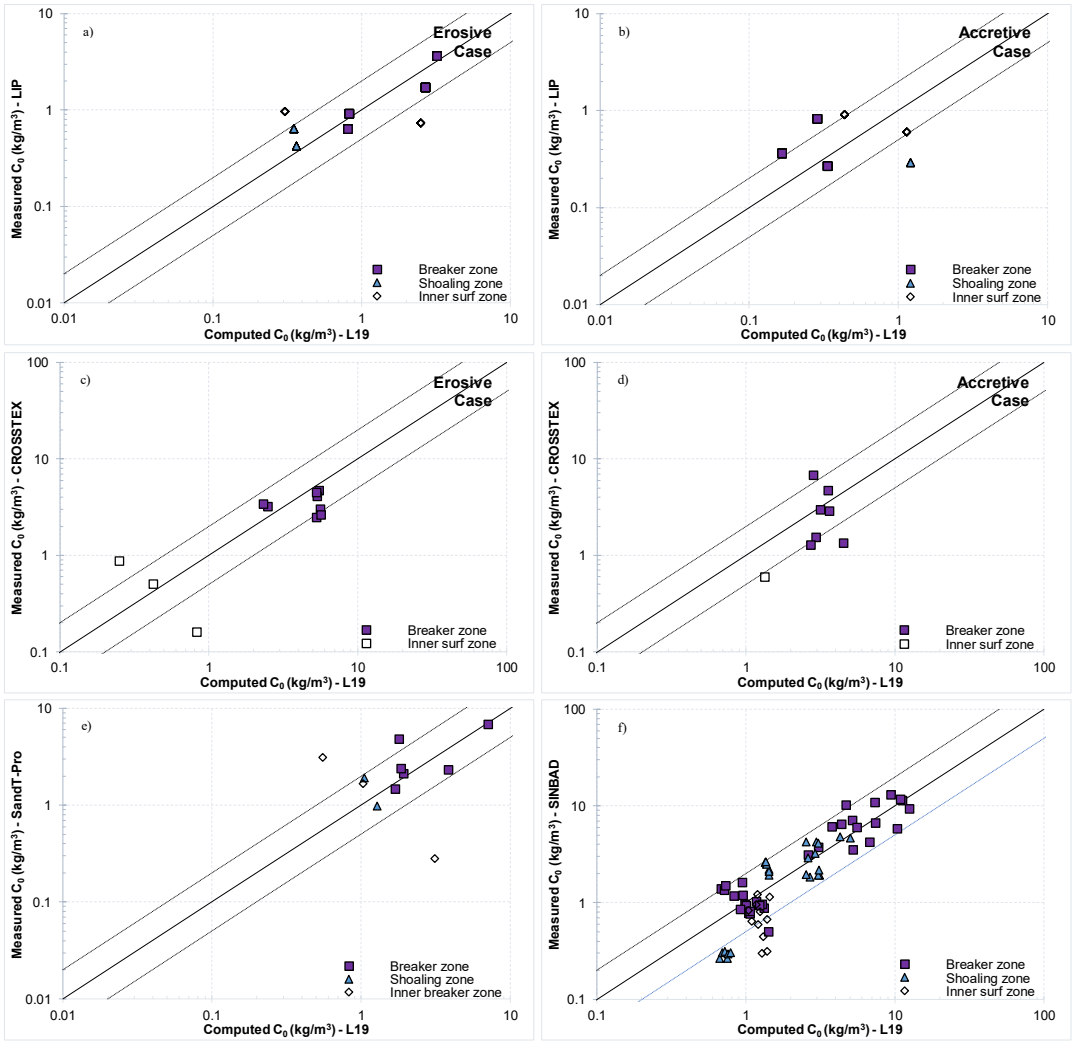

Figure 19 – Measured vs. Computed reference concentration – derived using the model of L19. Plot a-b show the L19 model validated against LIP erosive and accretive conditions respectively; c-d show validation against CROSSTEX erosive and accretive conditions respectively; e-f show validation against the SandT-Pro and SINBAD experiments respectively.

LIP & CROSS: The L19 model performs very well in all three regions, including the breaking region for the erosive and accretive cases (note: 1 point is not shown in Fig 19b as it was an outlier located far outside the plot range). In the accretive case of CROSSTEX (Fig.20d), L19 shows good agreement at the plunging point, but is seen to under-predict slightly immediately shoreward of the plunging point – as seen against the SINBAD dataset (Fig.20f).

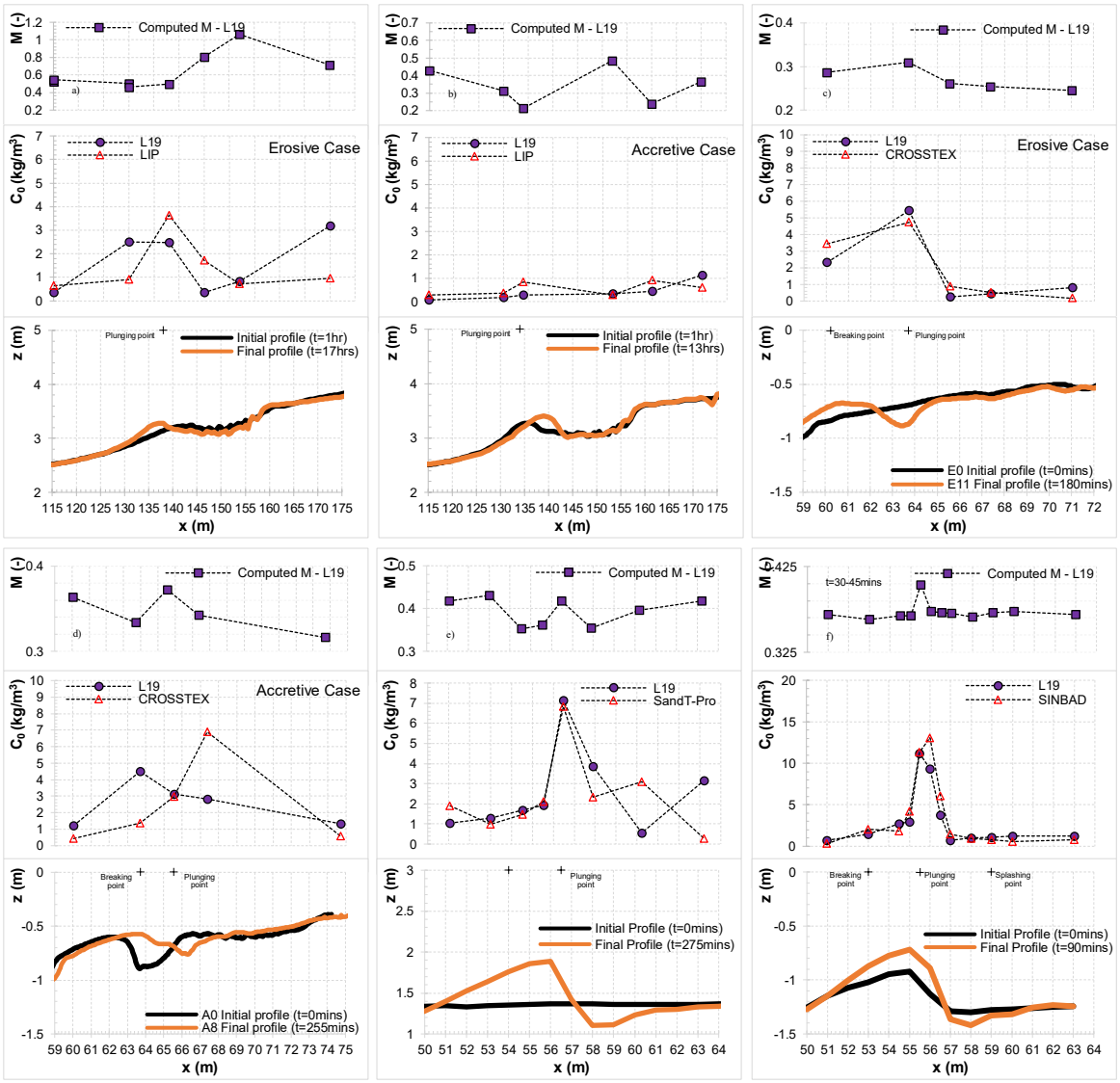

Figure 20 – Cross-shore distributions of mixing parameter (top panels), measured and computed reference concentration (middle panels) and bed profile (lower panels). Plots a-f show the L19 model validated against each of the datasets LIP erosive and accretive cases, CROSSTEX erosive and accretive cases, SandT-Pro and SINBAD respectively.

SandT-Pro & SINBAD: L19 shows good agreement with the measured C_0 in the shoaling and breaker zones - considerably better agreement than other existing models - with RMSE = 1.58kg/m^3 for SandT-Pro (see Table 5). Figs.19e-f show that almost all points are clustered around the 1:1 line and lie within the factor of 2 region. Even when the breaker bar is fully developed at t=90mins, the L19 model accurately captures the localised increase in C_0 at the plunging point, as well as maintaining good agreement with data in other zones. In Fig.20f, there is some divergence just shoreward of the plunging point, between x=55-56m. The bottom profile in Fig.20e-f, shows that the bed level drops at this location. As the inverse of the water depth ($1/d$) is one of the main driving parameters of the L19 model, the fall in the bottom profile between x=55m and x=56m is reflected in the corresponding computed C_0, which also drops with the bed profile. The measured C_0 at this point however increases. This is attributed to the strong turbulent vortices fully invading the WBBL at this point, entraining large

amounts of sediment as well as enhancing vertical mixing. The L19 model does not account for the oblique downward movement or enhanced mixing effects of these turbulent vortices which continue to move towards the bed beyond the plunging point. The lag involved in the TKE travelling through the water column, as well as TKE being horizontally advected to/from adjacent regions is also not accounted for in the model. Instead it models the reference concentration empirically from the local water depth and roller dissipation rate. As a result, though L19 is adept for predicting C_0 at the plunging point, it is sometimes seen to under-predict immediately shoreward of the plunging point.

There are also some cases of noticeable over-predicting in the inner surf zone (particularly observed in Fig.20a & 20e when validated against the LIP erosive and SandT-Pro datasets). As mentioned in section 2 of this report, the observed inverse relationship between local water depth and corresponding C_0 is only applicable up until the plunging point (x=138m and x=56.5m for LIP and SandT-Pro datasets respectively). Figures 20a & 20e show that the agreement between computed and measured C_0 is very good up until this point, but afterwards there are some discrepancies.

Summary: The model of L19 generally performs very well in all three cross-shore regions, but especially in the shoaling and breaking zones. Unlike the other existing reference concentration models validated in this study, the L19 model is adept at capturing the strong localised increase in C_0 found at the plunging point. Immediately shoreward of the plunging point however, where SSC peaks due to the large-scale vortices fully invading the WBBL, the model is sometimes found to under-predict marginally. Overall however, the model accurately reproduces the cross-shore variability of reference concentration under plunging breaker conditions.

Table 5 – Summary of RMSE for all reference concentration models tested against measured data. The lowest RMSE (best agreement with measured data) in each dataset is highlighted in bold.

Model	**SandT-Pro**	**SINBAD**	Erosive **CROSSTEX**	Accretive **CROSSTEX**	Erosive **LIP**	Accretive **LIP**
MS92	3.41	8.08	2.75	4.54	1.89	4.57
SR93	2.61	3.45	2.35	2.79	1.12	0.61
SP04	3.61	4.13	1.47	3.81	1.44	0.52
JS07	2.49	4.43	**1.70**	2.33	1.92	3.72
VR07	2.85	7.43	-	-	3.28	10.47
vdZ17	-	5.02	2.30	2.58	-	-
L19	**1.58**	**1.42**	1.71	**1.79**	**0.75**	**0.36**

4.2 Concentration Profile

The concentration profiles shown in Fig.21 indicate a similar pattern over the cross-shore regions. Throughout Fig.21, plots on the left show the concentration profile prior to wave plunging, the centre plots show concentration at plunging point and the plots on the right show concentration post-plunging. Generally, prior to plunging, concentration levels are relatively low, in the order of 10^{-1} kg/m^3. At this point, MS92 and SR93 show good agreement with measured data throughout the whole water column. Both MS92 and SR93 are driven (in part) by the Shields Parameter, which assumes entrainment occurs when local bed shear exceeds critical bed shear. This suggests that local TKE induced by bed shear is dominant in this region and that the Shields Parameter is adept for capturing the low levels of concentration in the shoaling zone. This is not adequately modelled by the model of van Rijn (2007) however, showing considerable over-prediction pre-plunging (e.g. Fig.21j and Fig.21p). L19 also consistently yields good agreement with measured data throughout the water column pre-plunging. This indicates that the inverse relationship between local water depth and reference concentration (Eq.19) is valid in the shoaling zone. The SP04 and JS07 models, which are both driven by local and/or breaker wave height (H or H_b), are often shown to over-predict considerably in the shoaling zone (e.g. Figs.21m & 21p). Figure 12 indicates that H and H_b show a weak correlation with the reference concentration, suggesting that wave height is not a good driver for reference concentration in the shoaling zone.

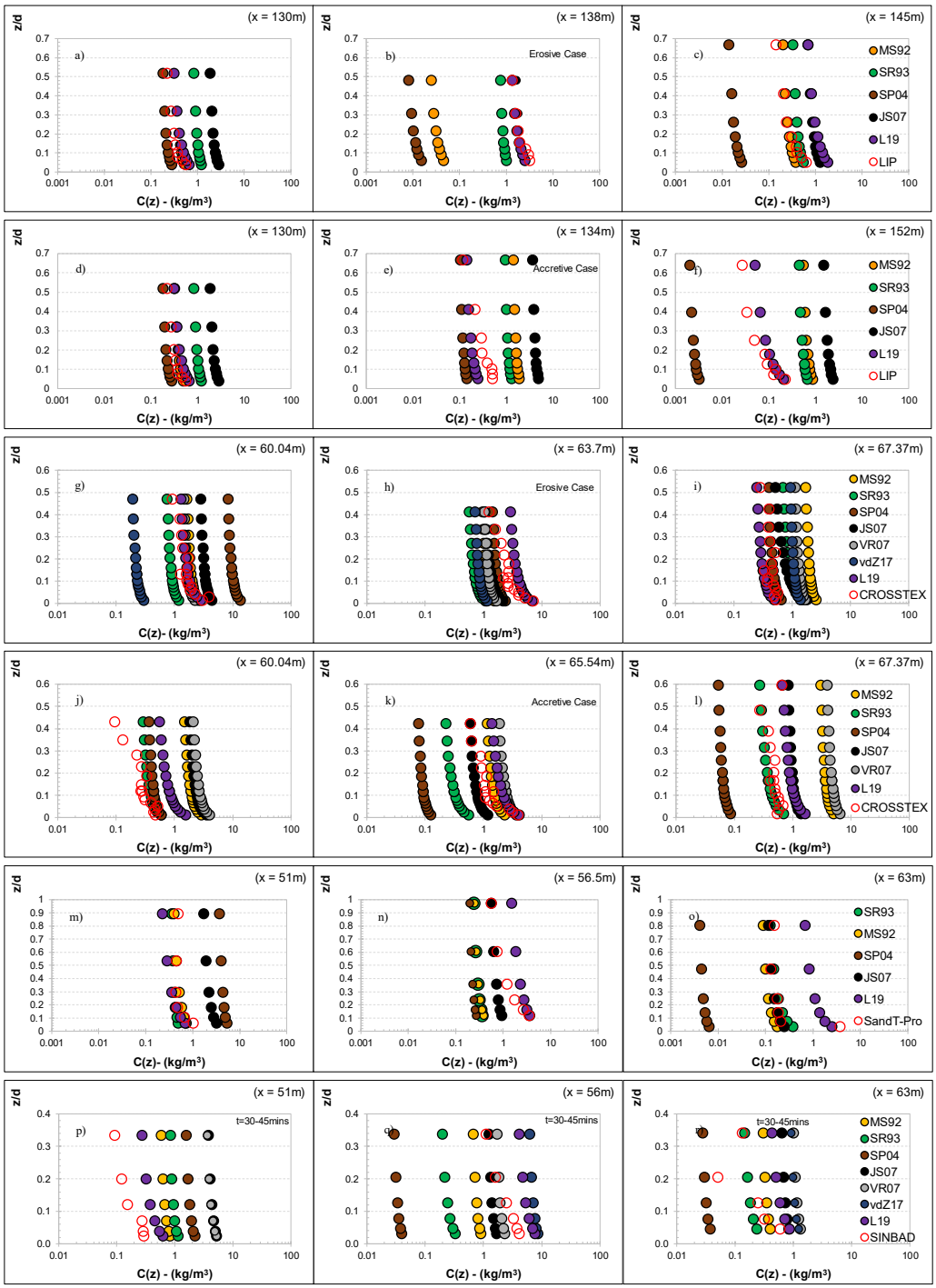

Figure 21– Concentration profile [$C(z)$] of Measured vs. computed concentration. Plots a-c show LIP erosive and d-f show LIP accretive cases respectively; plots g-i show CROSSTEX erosive and j-l show CROSSTEX accretive cases respectively; plots m-o show are SandT-Pro and plots p-r are SINBAD. Each row of plots shows three different cross-shore locations: before the breaking point (left plots), at the breaking or plunging point (central plots) and onshore of the breaking point (right plots).

In the breaking region, MS92, SR93, SP04, VR07 and in some cases JS07 as well, are generally shown to under-predict concentration, especially in the near-bed region ($z/d < 0.2$) as seen in section 4.1. It is clear that wave breaking has a considerable effect on sediment pickup rates as well as the reference concentration, which is evidently larger by one order of magnitude in the breaking zone than the shoaling zone (e.g. vdZ et al. 2017a). Assuming the magnitude of near-bed TKE is correlated with the magnitude of sediment pickup rates, this is also consistent with the findings of Scott et al. (2005) who reported that levels of near-bed TKE were an order of magnitude higher at the bar crest (generally where waves break) than in the shoaling and inner surf zones. The concentration profiles show that sediment concentration doesn't only increase near the bed in the breaking zone but increases throughout the whole water column. vdZ et al. (2016) reported that TKE is almost

depth-uniform in the vicinity of the plunging point, and this is reflected in the high concentration in the full water column. This phenomenon is attributed to strong vertical mixing by the breaking-generated turbulent vortices, rising air bubbles (as described in section 1) and also upward advection by two-dimensional undertow circulation (Fernandez-Mora et al., 2016; vdZ et al. 2017a). This strong vertical mixing (most evident in Figs.21n & 21q) is not well captured by the any of the tested models, often showing discrepancies higher up in the water column, even when agreement is good in the lower water column. As the majority of the concentration profiles were computed using Eqs.23-24, this suggests that Eqs.23-24 do not sufficiently account for the strong mixing and vertical advection induced by turbulent vortices and undertow circulation. Agreement between L19 and the measured concentration profile is still generally good, particularly in the near-bed region. The magnitude of sediment concentration declines substantially from the breaking to the inner surf zone, particularly in the upper water column ($z/d > 0.2$). As the sediment concentration decreases from the breaking zone to the inner surf zone, the models are found to perform better. There are however cases of under-prediction with instances of high concentration still remaining in the WBBL (e.g. Figs.21o & 21r). This residual turbulence could be attributed to the secondary wave (vdZ et al., 2016) or surface bores which were reported to be dominant in the inner-surf zone (Brinkkemper et al., 2016).

5. Discussion

5.1 General limitations of existing C_0 models

Local wave climate and water depth

As mentioned briefly in section 1 of this report, accurately predicting the reference concentration under breaking wave conditions has been the focus of numerous studies. The analysis carried out in section 4 has provided some insights into the various strengths and weaknesses of previous endeavours, as they were validated against four datasets measured under large-scale wave breaking conditions. One of the most commonly observed limitations was found in models (e.g. MS92, SR93, SP04 and JS07) that were dependant on or driven by the wave height (H and H_b) and/or local water depth (d). As identified in section 4.1 (refer to Fig.12), the measured H, H_b and d did not correlate well with reference concentration, especially at the plunging point where these parameters were often seen to decline in magnitude whilst corresponding measured C_0 largely increased. This finding is in agreement with those of vdZ et al. (2017b) who also reported poor correlation between the local wave climate and the strong localised increases in reference concentration observed at the plunging point. The models of MS92 and SR93 which were largely driven by H and d, produced cross-shore C_0 distribution that mirrored the cross-shore distributions of H and d, with computed C_0 declining at the plunge point. Consequently, these models were not able to capture the high localised increase in C_0 post-plunging (see Figs.7, 9, 11 and 14) and were generally found to under-predict throughout the breaking region.

The MS92 and SR93 models were however adept in predicting the reference concentration in the shoaling and inner surf zones. The model validation in section 4.1 has indicated that models that have related the reference concentration with the sediment pickup rate (formulations that depend on local bed shear levels exceeding critical bed shear for entrainment; formulations driven by the Shields Parameter) are quite capable of modelling reference concentration in regions and/or conditions that are predominantly influenced by local TKE induced by bed shear (e.g. the shoaling region or non-breaking conditions). These formulations however are often based on the implicit assumption that sediment entrainment is only affected by the local TKE induced by bed shear (e.g. van Rijn, 1984; 2007). Though this assumption is applicable to non-breaking conditions or in the shoaling zone, as reported by vdZ et al. (2017b), this assumption is no longer valid when the external breaking induced TKE invades the WBBL. This is consistent with Aagaard et al. (2018) who inferred that sediment concentration, or sediment pickup models based on bed shear stress derived from horizontal velocities would be unsuitable for breaking wave conditions. In response, vdZ et al. (2017b) proposed an adapted transport parameter that considers the near-bed TKE (k_b) induced by both internal (local) and external (surface/breaking-generated) TKE. This new formulation was derived based on the causal relationships observed between k_b and C_0, suggesting that when k_b exceeded the critical bed shear level, sediment would be entrained. An advantage of using near-bed TKE to drive sediment concentration and pick-up rate models is that it allows the model to account for breaking induced turbulence which spreads through advection and diffusion processes, both vertically and horizontally (vdZ et al. 2016; 2017a,b). It could be important to incorporate such processes in concentration formulae as they are responsible for increased levels of k_b and sediment entrainment not only in the breaking region, but also in neighbouring locations (vdZ et al. 2017a). Such advection and diffusion processes are accounted for in models driven by k_b, but not in the other existing models covered in this study.

Near-bed TKE

As seen in Fig.18, the model of vdZ17 shows varied performance when validated against the different datasets. In section 4.1, it was briefly mentioned that the near-bed TKE measurements (at 1cm above bed) varied in magnitude between the CROSSTEX and SINBAD experiments. For further comparison of the measured TKE values between the two experiments,

the Froude-scaled TKE $(k/gh)^{1/2}$ was computed. The $(k/gh)^{1/2}$ levels found at ≈1cm above the bed in the spilling/plunging region, in both the erosive and accretive cases of the CROSSTEX experiments, were found to be between 0.021-0.032, whereas in the SINBAD experiments, they were between 0.027-0.035. It is speculated that the differences in the magnitude of TKE measurements could be a result of several factors. vdZ et al. (2016) used a Reynolds decomposition based on the ensemble-averaging method, and Yoon & Cox (2010) used a differencing method to separate the wave-related components from the turbulence-related components of velocity. Scott et al. (2005) carried out analysis on three methods of extracting TKE from the velocity data (high-pass filtering, ensemble-averaging and differencing method) and reported that the different methods yield different estimates of TKE. It was found that for regular waves, the TKE estimates from the differencing method were larger than the estimates from the ensemble-averaging method by approximately 26% (Scott et al., 2005). This is inconsistent with the trend observed in Fig.22 which shows that the values from the ensemble-averaging method yield higher values of $(k/gh)^{1/2}$. Assuming that the small difference in offshore conditions of the experiments are negligible (see section 3 for details on offshore conditions), this suggests that the difference in magnitude of measured TKE is not a result of the method of extracting turbulence measurements.

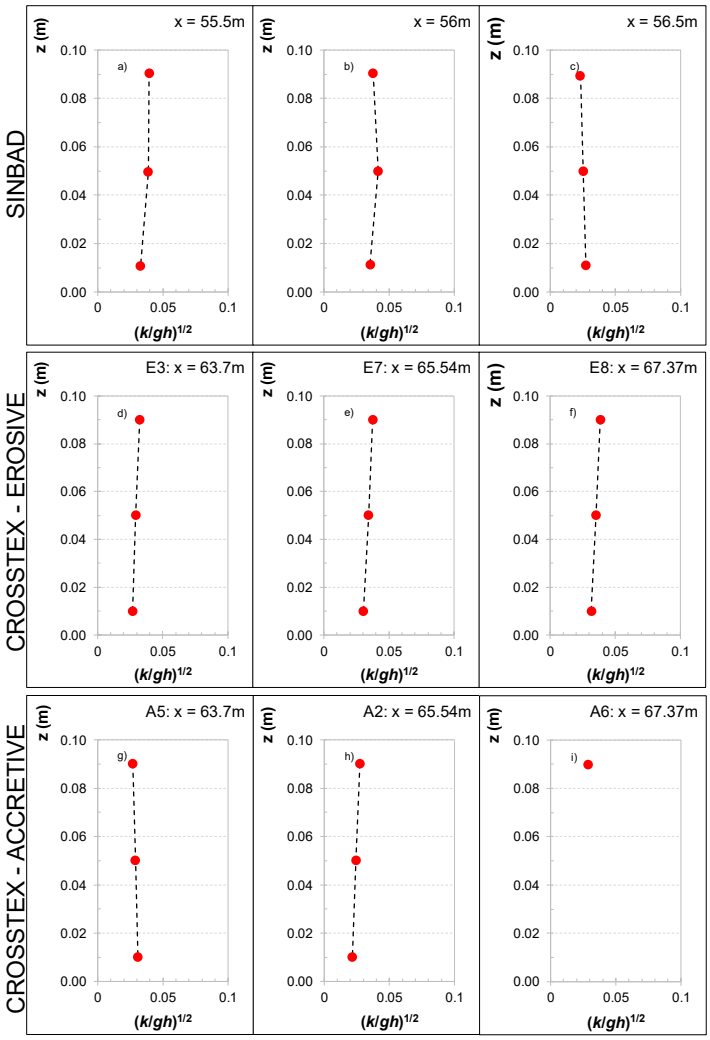

Figure 22 – Vertical profile of Froude-scaled TKE at 1cm above the bed from the SINBAD and CROSSTEX datasets. Plots a-c) show TKE at three cross-shore locations, at the breaking point, at the plunging point and onshore of the plunging point. Plots d-f) and plots g-i) show TKE at three cross-shore locations, at the breaking point, at the plunging point and onshore of the plunging point, for erosive and accretive conditions respectively.

On the other hand, though the turbulent structure was reported to be the same in both the regular and irregular wave conditions, the magnitude of TKE was found to be considerably smaller in the irregular/random cases – up to a factor of 5 (Scott et al., 2005) despite similar offshore wave conditions. This finding is more consistent with the trends observed in the present study. As described by Scott et al. (2005), the vertical turbulence structure observed in Fig.22 between the two experiments are similar despite the difference in wave conditions. Also, the Froude-scaled TKE measurements from the CROSSTEX experiments (irregular waves) are smaller by approximately a factor of 1.1-1.3. This suggests that the difference in trends

observed between the two experiments could be a result of the wave conditions as the SINBAD experiments were carried out in regular, and the CROSSTEX in irregular wave conditions. There were also differences in bottom profile and breaker bar development between the two experiments, which could also have had an effect on the difference in magnitudes of k_b and $(k/gh)^{1/2}$ between the two experiments.

Though a strong relationship between near-bed TKE and reference concentration is well validated, it can clearly be seen that there are some inherent challenges in using k_b as the primary driving parameter for reference concentration models. These challenges range from choosing the best method of extracting turbulence from data, to the effects of the wave conditions (e.g. regular/irregular) and the bottom profile on the magnitude of TKE. It is also reported that there are numerous difficulties in the accurate modelling of the spatial trends and magnitude of near-bed TKE, even with high-resolution state-of-the-art CFD models (vdZ et al. 2017b, Fernandez-Mora et al., 2016).

Based on the observations in TKE magnitude, in both k_b and $(k/gh)^{1/2}$, the deviation between values from the different datasets is smaller in the Froude-scaled turbulence. This suggests that $(k/gh)^{1/2}$ may serve as a better driver for reference concentration than k_b, which fluctuates more between datasets. This is supported by Aagaard et al. (2018) who reported that for intense suspension events (such as those found under the plunging breakers observed in this study) Froude-scaled instantaneous TKE shows good agreement with instantaneous sediment concentration, for both plunging and spilling breakers.

5.2 Application to morphodynamic models

One of the issues in using process-based morphodynamic models (such as Delft3D, MIKE21 and Telemac) for long-term modelling is the lack of accuracy and/or robustness of constituent sediment transport models. This problem stems from limited understanding and insights into sediment transport processes and how they interact with complex hydrodynamic forcing – e.g. under breaking wave conditions. As such, until further insights and detailed understanding is obtained and implemented into more process-based models, even in the aforementioned state-of-the-art process-based morphodynamic modelling suites it is often necessary to rely on engineering or 'practical' models which incorporate relatively simpler physics with (semi-)empirical parameterisations. The various models covered in this study, including the L19 model can more or less be categorised as practical models. These practical models are not only useful but somewhat necessary in reducing computation times whilst maintaining modelling accuracy – benefits that are particularly valuable in modelling sediment transport and resulting morphology for medium- to long-term periods. Such benefits can also help researchers to obtain insights into poorly understood phenomena and processes by carrying out much needed (sensitivity) analysis to identify key parameters and causal relationships between inherent processes.

Systematic validation (and development) of existing and new practical transport models using latest observational insights and data (as done in the present study) is essential in understanding the limitations of existing models and improving them for use in morphodynamic modelling. For example, many of the existing models in the present study (e.g. the van Rijn, 2007 formulae which are widely used in existing morphodynamic models) were found to under-predict the suspended load considerably, particularly in the breaking zone (see section 4). Such under-prediction of the suspended load can lead to imbalances between the suspended load transport and bedload transport which often occur in opposite directions, resulting in unrealistic net transport rates. Even if these errors are relatively small and negligible in the short-term, they can accumulate over the long-term to produce inaccurate predictions of morphological changes. As such, it is important to implement improved suspended load models and methods that are robust and accurate into morphodynamic models. Based on the results of the present study it is speculated that the implementation of the newly developed L19 formula into existing morphodynamic models could enhance performance (in terms of accuracy of predictions and lower computational costs) and is the focus of an ongoing concurrent study.

Applicability to multiple cross-shore zones

The practical reference concentration models evaluated in this study can be put into two categories regarding applicability to multiple cross-shore zones: 1) models that do not require additional formulae or changes in parameters/constants for implementation to multiple cross-shore regions, and 2) models that do require additional formulae or changes. For example, models that utilise a transport parameter that is based on the Shields Parameter or sediment pick-up rate (e.g. MS92, SR93, VR07 and vdZ17) do not need to be able to distinguish which cross-shore zone they are being applied to. I.e. the parameters or constants used in the formulations do not change based on the cross-shore region (category 1). Models such as JS07 and the proposed L19 model fall into category 2 and are affected by the cross-shore region, requiring additional formulae/parameters depending on the regions they are applied to. The reference concentration models in category 1 were often found to perform quite poorly in the present study when applied to the different cross-shore regions, generally only being adept for one or two cross-shore regions at most. Analysis from section 4 showed that the tested models performed particularly poorly in the

breaking zone under strong plunging breakers. It is suggested that the inclusion of additional formulae or (tuning-)parameters to the models in category 1 could help to improve their overall performance in all cross-shore zones. For example, a model that is adept for performance in the shoaling and inner surf zones but performs poorly in the breaking zone could include a tuning (or additional) parameter or alternative formulae to improve agreement with measured data in the breaking zone. Examples of this can be found in the work of Jayaratne & Shibayama (2007) and also the newly proposed L19 formulae.

As mentioned in section 4.1, the JS07 model was derived for predicting SSC under breaking agitation only. Because the original C_0 formulation of JS07 was derived for use in the breaking zone only, parameters such as H_b, d_b and L_b were used, where the subscript b denotes at the breaking point. However, from a practical point of view, there are limited uses for a reference concentration model that can only be used (adeptly) for the breaking zone. For this reason, in order to test the model's applicability to other cross-shore regions, the authors carried out the validation using local wave height (H) instead of breaker height (H_b), local wavelength (L) instead of breaker length (L_b) and local water depth (d) instead of the water depth at the breaking point (d_b). As presented in section 4.1 and 4.2, despite being derived for the breaking zone only, the JS07 model often performs reasonably when driven by local measurements, especially in the inner-surf zone and also in some cases in the breaker zone. Jayaratne & Shibayama (2007) also derived separate models for the various suspension mechanisms observed in breaking and non-breaking wave conditions. Three models were produced for each of the following mechanisms: 1) suspension due to rippled-bed, 2) due to sheet-flow and 3) due to wave breaking agitation (JS07 model covered in present study). When the models of Jayaratne & Shibayama (2007) are applied to the shoaling zone where sheet-flow conditions are prevalent (Ribberink et al., 2014; vdZ et al. 2018; Fromant et al. 2019), the reference concentration formula for sheet-flow conditions should be applied, and in the breaking zone the model for breaking agitation should be applied and in the inner surf zone where vortex ripples are present (e.g. vdZ et al., 2016), the model for rippled bed conditions could be applied. Jayaratne & Shibayama (2007) also derived formulae to predict the concentration under the combined effects of ripples and breaking agitation – two suspension mechanisms that often occur in the same phase, as in some regions multiple suspension mechanisms will coexist. By implementing the multiple-formulae method of Jayaratne & Shibayama (2007), the suspended load can accurately be modelled in all cross-shore regions by applying the ideal model(s) to each region.

Alternatively, the L19 model implemented a simple tuning parameter ω (see Eq.20) which empirically accounts for the combined effects of the different suspension mechanisms present in the various cross-shore regions (e.g. sheet-flow in the shoaling zone, entrainment resulting from wave breaking in the breaking zone). The L19 model has generally shown very good agreement with measured data in the shoaling and breaking zones but requires a different value of the constant ω to be implemented for the inner surf zone. In cases where the boundaries for the cross-shore regions have been clearly established, it is possible to manually (or by programming) implement the new ω value for the shoaling zone, for example when running morphology simulations. When only computing the reference concentration for short-term laboratory experiments or micro-scale morphology (e.g. temporal scale of minutes to hours; spatial scale of metres), manually implementing the desired formula or constant (such as ω) for the different cross-shore zones is straightforward. However, when such formulae are integrated into morphology models for medium- to long-term simulations, it would be necessary to set explicit boundary conditions based on measured or modelled parameters to differentiate between the different zones (e.g. assuming local water depth d = 2m at the boundary between breaking and inner surf zone, when $d \geq$ 2m then ω = 7.5 and when d < 2m, ω = 1.0). This would ensure smoother simulations and be more efficient, especially in tests involving large amounts of data (e.g. medium- to long-term large-scale morphology).

In cases where the cross-shore regions have not been explicitly distinguished, implementing the different ω values for different cross-shore zones could be more challenging. In the work of vdZ et al. (2016), the different cross-shore regions were identified by examining the phase-averaged measurements of the water surface elevation. Based on these observations and the work of Svendsen et al. (1978), the three cross-shore zones were distinguished. Where surface elevation measurements are available, such analysis can be carried out to establish the various cross-shore regions. The boundary between the breaker and inner surf zone also seems to be qualitatively distinguishable in terms of the wave climate (e.g. local wave height) or the local water depth in the datasets described in section 3 of this report (see also Fig.12 and cross-shore profile evolution in Figs.1-5). The experimental datasets described in section 3 show that the cross-shore distribution of H and d recede from the shoaling region to the breaking region. vdZ et al. (2016) reported that the wave energy dissipation in the SINBAD experiments started at the breaking point, and continued through the breaking zone, with local wave height declining by 50% between the shoaling and inner surf zone. This is somewhat consistent with observations in the other datasets which indicate that H continues to fall until the plunge point, after which it increases marginally before falling again. It is speculated that this momentary marginal increase in H indicates the small wedge of water pushed up by the plunging jet which then forms a secondary wave (vdZ et al. 2016). The water depth d falls until the plunge point, where the breaker trough is located. At this point d begins to gradually rise again momentarily, before declining once more as the inner surf zone gives way to the swash zone. From these observations of H and d, and/or observations of the water surface level, as described by vdZ et al. (2016), the various cross-shore regions can be identified. These methods, among others, suggest that models such as JS07 or L19, that require the distinguishing of

cross-shore zones, are applicable to morphology models.

It should be noted however that the present observations are based on controlled prototype scale laboratory experiments and may differ from observations in the field. As such, the distinguishing of cross-shore zones may require more detailed examination of hydrodynamic processes. The scope of the present study however does not extend into the hydrodynamic processes that are involved in distinguishing cross-shore zones. The authors speculate however that such research could be invaluable in the integrating of more accurate SSC models into morphology models and would recommend a more detailed analysis of the hydrodynamic processes observed in the different cross-shore regions in future studies. Section 4 of this study has clearly indicated that the existing reference concentration models are not perfectly adept for use in all (multiple) cross-shore zones and transport mechanisms and as such, the recommended research could allow for separate (or a combination of) models or parameters that are idealised for specific cross-shore zones or sediment transport mechanisms (similar to the approach of Jayaratne & Shibayama, 2007) to be used in conjunction, rather than a one-size-fits-all model that is used for all cases.

For whatever reason, the situation may require the user to use a one-size-fits-all formula or constant (like those in category 1). The L19 model generally performed very well in all cases when using a varying ω parameter, but there were some (often quite large) discrepancies found in the inner surf zone. If a constant value of ω was to be used in all cross-shore regions, the level of accuracy could be forfeited (albeit marginally) for gain in computational efficiency. Depending on the constant value of ω selected, the accuracy of the model can vary considerably. Using ω = 7.5-15 (recommended values for shoaling/breaking zones, suggested in section 2.1) in all three zones would ensure good agreement in the shoaling and breaking zones, as observed in section 4, but result in over-prediction in the inner-surf zone. Through sensitivity analysis, this over-prediction in the inner-surf zone was found to be as little as ≈1.5 kg/m^3 (still in the correct order of magnitude) and as large as ≈18 kg/m^3 (one order of magnitude higher than measured). Using ω = 1.0-3.0 (recommended values for inner surf zone, suggested in section 2.1) for all zones will ensure good agreement with data in the inner-surf zone, but substantial under-prediction in the shoaling and breaker zones. If a constant value of ω is to be used for all zones, the authors would recommend a value of ω = 7.5, based on the results of the sensitivity analysis (not shown).

Regardless of the value(s) of ω selected, and the method of implementation into morphodynamic simulations, the introduction of the omega constant provides a novel solution to the problem of differing processes in different cross-shore regions. The proposed L19 model is robust and simple, consisting of only a few parameters that do not require complex calculations, with all key driving parameters easily measured or computed using common wave theories. It has also indicated good accuracy in all investigated cross-shore regions and is therefore deemed well-suited for implementation into morphodynamic models.

5.3 Applicability to irregular wave conditions

Erosive and Accretive

Though the new L19 model has proven to perform very well under regular waves in controlled laboratory experiments (e.g. against the SINBAD and SandT-Pro datasets), it is also necessary to evaluate its applicability to field-scale random or irregular waves if the model is to be used practically in the field. As mentioned in section 5.1, though there are considerable differences in the magnitude of measured k_b, the general TKE structure and hydrodynamics remain similar between regular and irregular wave conditions (e.g. Scott et al., 2005; Brinkkemper et al., 2016). As a result, the existing models evaluated in this study show similar performance in both regular and irregular conditions, with substantial under-predicting found at the breaking/plunging points. It should be noted however that the random waves break over a wider cross-shore area than in regular wave conditions, making it difficult to pin-point one location as the breaking or plunging point. This is supported by the findings of Scott et al., (2005) who reported that the surf zone created under irregular waves was broader than that found under regular cases, with a larger percentage of waves not breaking over the bar but propagating over the bar without breaking. It is speculated that these waves could have broken further onshore. This is consistent with Yoon & Cox (2010) who reported that waves generally broke at the bar crest, but as time progressed in the accretive runs, the bar decayed, and more waves passed over the bar, breaking later in the surf zone. As such, the points labelled breaking and plunging point in the CROSSTEX and LIP conditions are only estimations based on bottom profile evolution and measured TKE observations and the reports of the original authors. Based on the consistency of observed trends between computed and measured C_0 and measured TKE however, these estimations of breaking and plunging points seem reasonable.

Despite the irregular wave conditions, the L19 model agreement is generally very good. As the model is not driven by the local wave- or current-related velocity or k_b, it is not majorly affected by the differences in hydrodynamic conditions between regular and irregular wave conditions. As it can be seen in Fig.12, the proposed empirical relationship between the inverse water depth ($1/d$) shows good agreement with measured reference concentration throughout the shoaling and breaker zones

for both regular and irregular wave conditions. Generally, the reference concentration models covered in this study performed better under erosive conditions than accretive conditions. Accretive conditions are associated with low- to moderate-wave energy conditions with relatively long wave periods (Aagaard & Hughes, 2010). This suggests that the tested models are more adept for erosive, medium- to high-energy wave conditions with shorter wave periods.

6. Conclusions

A total of 7 reference concentration models (6 existing and 1 newly proposed) were evaluated for performance in different cross-shore regions – shoaling zone, breaking (outer surf) zone and inner surf zone – under regular and irregular breaking wave conditions. These reference concentration models were validated against four recently published datasets collected under the LIP, CROSSTEX, SandT-Pro and SINBAD experimental studies.

Generally, models driven directly or indirectly by local wave climate such as the wave height (H), breaker height (H_b) or local water depth (d), were found to perform quite poorly in the breaking region. This was especially the case around the plunging point where there was a strong localised increase in C_0, attributed to the large breaking-generated turbulent vortices invading the WBBL and entraining dense clouds of sediment. Corresponding H, H_b and d were found to be lowest at this point, causing formulations driven by these parameters to under-predict. This was a problem that was found to affect 4 out 7 of the evaluated models: MS92, SR93, SP04 and JS07. Of the affected models however, the models that related reference concentration to the sediment pickup rate (depending on local bed shear exceeding critical bed shear for entrainment) were adept in regions unaffected by external breaking-induced TKE (e.g. the shoaling zone, and also in some cases the inner surf zone where there are lower levels of near-bed TKE) but were not able to account for the strong localised increase in C_0 observed at the plunging point. This is because these formulations are based on the implicit assumption that sediment entrainment is only induced by the local TKE generated by bed shear. This assumption is only valid in regions where surface-generated TKE is not present. A potential solution to this problem is the inclusion of breaking-induced TKE into the sediment pickup rate or reference concentration formulations. There are however several challenges involved with this method. Though recent studies have shown promising relationships between near-bed TKE (k_b) and reference concentration/sediment pickup, such formulations are highly dependent on the accuracy of measured or modelled k_b. Accurately predicting the spatial trends and magnitudes of near-bed TKE is very difficult. Also, analysis carried out in sections 4.1 and 5.1 indicated that the magnitude of TKE found in regular and irregular wave conditions differ considerably, with TKE found under regular waves being larger by up to a factor of 5 in existing literature. Such differences in magnitude of k_b can have major effects on models driven by near-bed TKE. Based on sensitivity analysis, it was proposed that Froude-scaled TKE $(k/gh)^{0.5}$ may be a more suitable driver than k_b for such formulations.

The newly proposed L19 model is not affected by such limitations, showing good agreement with measured C_0 in regular and irregular wave conditions, even at the plunging point where concentration is highest. The modified mixing parameter produces improved concentration profile [$C(z)$] predictions, generally capturing the vertical concentration profile accurately throughout the water column. The mixing parameter can also be seen to reflect the high levels of sediment mixing expected at the plunging point. As the L19 model is empirical, depending largely on the inverse relationship between local water depth and C_0, it does show some discrepancies in the inner surf zone where the inverse relationship is no longer applicable. A new value for the constant ω is introduced for the inner surf zone, reducing discrepancies between computed and measured C_0. In practise, for example when used in morphology models, the boundary between the outer surf zone and inner surf zone (i.e. the point where the value of ω must be changed) can be identified qualitatively or quantitatively by studying the water surface elevation or the cross-shore variability of H and d. The ω constant provides a novel solution to incorporating the different prevalent processes (e.g. different sand suspension mechanisms) that occur in different cross-shore regions, allowing for one single formula to be used for all cross-shore regions rather than, say, one formula for each zone. The model is also adept for irregular wave conditions as well as regular wave conditions making it suitable for field application. The simple and robust L19 model is applicable to morphology models and also deemed ideal for longer simulations that require minimal computational costs (e.g. long-term morphology).

Acknowledgements

This work was supported by the University of East London (UEL) under the UEL's Excellence PhD Studentships Scheme 2017-18. The authors would like to acknowledge Waseda University as collaborators in this project. Special thanks are given to Joep van der Zanden of the Maritime Research Institute Netherlands for sharing experimental data and invaluable comments and insights for the present manuscript. The authors would like to thank Daniel Cox of Oregon State University and Hyun Doug Yoon of Myongji University for sharing their datasets with the authors. Finally, the authors would like to thank Harshinie Karunarathna of Swansea University and the two anonymous reviewers whose comments helped to improve the manuscript.

References

Aagaard, T. and Hughes M.G., 2010. Breaker turbulence and sediment suspension in the surf zone. Marine Geology 271, 250-259.

Aagaard, T., Hughes, M.G. and Ruessink, G., 2018. Field observations of turbulence, sand suspension and cross-shore transport under spilling and plunging breakers. Journal of Geophysical Research: Earth Surface. doi: 10.1029/2018JF004636

Aagaard, T. and Jensen, S.G., 2013. Sediment concentration and vertical mixing under breaking waves. Marine Geology 336, 146-159.

Beach, R.A. and Sternberg, R.W., 1996. Suspended-sediment transport in the surf zone: Response to breaking waves. Continental Shelf Research 16(15), 1989-2003.

Brinkkemper, J.A., Lanckriett, T., Grasso, F., Puleo, J.A. and Ruessink, B.G., 2016. Observations of turbulence within the surf and swash zone of a field-scale sandy laboratory beach. Coastal Engineering 113, 62-72.

Camenen, B. and Larson, M., 2008. A general formula for non-cohesive suspended sediment transport. Journal of Coastal Research 24(3), 615-627.

Deigaard, R., Fredsoe, J., 1989. Shear stress distribution in dissipative water waves. Coastal Engineering 13, 357–378.

Fernandez-Mora, A., Ribberink, J.S., van der Zanden, J., van der Werf, J. J., and Jacobsen, N.G., 2016. RANS-VOF modelling of hydrodynamics and sand transport under full-scale non-breaking and breaking waves. Proceedings of the 35th Conference on Coastal Engineering. Antalya, Turkey. https://doi.org/10.9753/icce.v35.sediment.29

Fromant, G., Hurther, D., van der Zanden, J., Van der A, D.A., Cáceres, I., O'Donoghue, T., and Ribberink, J.S., 2019. Wave boundary layer hydrodynamics and sheet flow properties under large-scale plunging-type breaking waves. Journal of Geophysical Research: Oceans, 124. https://doi.org/10.1029/2018JC014406

Grasso, F., Castelle, B. and Ruessink, G., 2012. Turbulence dissipation under breaking waves and bores in a natural surf zone. Continental Shelf Research 43, 133-141. doi: 10.1016/j.csr.2012.05.014

Hsu, T.J., and Liu, P.L.F. 2004. Toward modelling turbulent suspension of sand in the nearshore. Journal of Geophysical Research: Oceans, 109(C6).

Jayaratne, M.P.R. and Shibayama, T., 2007. Suspended sediment concentration on beaches under three different mechanisms. Coastal Engineering Journal, World Scientific 49(04), 357-392.

Kana, T.W., 1978. Surf zone measurements of suspended sediment. Proceedings of 16th Conference on Coastal Engineering, Hamburg, Germany, 1725–1743.

Kana, T.W., 1979. Suspended sediment in breaking waves; Tech. Report No. 18-CRD. University of South Carolina, Columbia, 153.

Mocke, G.P., and Smith, G.G., 1992. Wave breaker turbulence as a mechanism for sediment suspension. Proceedings of 23rd Conference on Coastal Engineering, Venice, Italy.

Mori, N., Suzuki, T., and Kakuno S., 2007, Experimental study of air bubbles and turbulence characteristics in the surf zone. Journal of Geophysical Research: Oceans, 112. doi:10.1029/2006JC003647.

Nadaoka, K., Hino, M. and Koyano, Y., 1989. Structure of the turbulent-flow field under breaking waves in the surf zone. Journal of Fluid Mechanics 204, 359-387.

Nairn, R.B., Roelvink, J.A., Southgate, H.N., 1990. Transition zone width and implications for modelling surf-zone hydrodynamics. Proceedings of 22nd Conference on Coastal Engineering, Delft, The Netherlands, 68–81.

Nielsen, P., 1984. Field-Measurements of Time-Averaged Suspended Sediment Concentrations under Waves. Coastal Engineering, 8(1), 51-72.

Nielsen, P., 1986. Suspended Sediment Concentrations under Waves. Coastal Engineering, 10(1), 23-31.

Ogston, A.S. and Sternberg, R.W., 2002. Effect of wave breaking on sediment eddy diffusivity, suspended-sediment and longshore sediment flux profiles in the surf zone. Continental Shelf Research 22(4): 633-655. doi: 10.1016/s0278-4343(01)00033-4.

Okayasu, A., 1989. Characteristics of Turbulence Structure and Undertow in Surf Zone, Doctoral Dissertation, University of Tokyo, 53-112.

Okayasu, A., Fujii, K., & Isobe, M. 2010. Effect of external turbulence on sediment pickup rate. Proceedings of the 32nd International Conference on Coastal Engineering, Shanghai, China.

Peregrine, D.H. and Svendsen, I.A., 1978. Spilling breakers, bores and hydraulic jumps, Proceedings of 16th Conference on Coastal Engineering 1, 540-550.

Rattanapitikon, W., and Shibayama, T., 1998. Energy dissipation model for regular and irregular breaking waves, Coastal Engineering Journal, 40(4), 327–346.

Roelvink, J.A., Reniers, A.J.H.M., 1995. LIP 11D Delta Flume experiments, A data set for profile model validation. Report H2130, Delft Hydraulics, The Netherlands.

Ribberink, J., Van der A, D., Van der Zanden, J., O'Donoghue, T., Hurther, D., Cáceres, I. and Thorne, P., 2014. Sandt-Pro: Sediment transport measurements under irregular and breaking waves, Proceedings of 34th Conference on Coastal Engineering, 1(34).

Sato, S., Homma, K. and Shibayama, T., 1990. Laboratory study on sand suspension due breaking waves. Coastal Engineering in Japan, 33(2), 219–231.

Scott, C. P., Cox, D.T., Maddux, T.B. and Long, J.W., 2005. Large-scale laboratory observations of turbulence on a fixed barred beach. Measurement Science and Technology 16(10): 1903-1912. doi: 10.1088/0957-0233/19/10/004.

Shibayama, T., and Rattanapitikon, W., 1993. Vertical distribution of suspended sediment concentration in and outside surf zone. Coastal Engineering in Japan, 36(1), 49–65.

Smith, G.G., & Mocke, G.P. 1993. Sediment suspension by turbulence in the surf zone. Proceeding of Euromech 1993, Le Havre, France.

Spielmann, K., Astruc, D., & Thual, O. 2004. Analysis of some key parametrizations in a beach profile morphodynamical model. Coastal Engineering, 51(10), 1021-1049.

Sumer, B.M., Guner, H.A.A., Hansen, N.M., Fuhrman, D.R. and Fredsøe, J., 2013. Laboratory observations of flow and sediment transport induced by plunging regular waves. Journal of Geophysical Research: Oceans 118(11): 6161-6182. doi: 10.1002/2013jc009324.

Svendsen, I.A., Madsen, P.A. and Buhr Hansen, J., 1978. Wave characteristics in the surf zone. Proceedings of 16th Conference on Coastal Engineering, 520-539

Svendsen, I.A. 1984. Wave Heights and Setup in a Surf-zone. Coastal Engineering 8, 303-329.

Swart, D.H., 1974. Offshore sediment transport and equilibrium beach profiles. Delft Hydraulic Lab., The Netherlands, 131, 1–244.

Thornton, E.B. and Guza, R.T. 1983. Transformation of wave height distribution. Journal of Geophysical Research 88(C10), 5925. doi: 10.1029/JC088iC10p05925.

Ting, F.C.K. and Kirby, J.T., 1994. Observation of Undertow and Turbulence in a Laboratory Surf Zone. Coastal Engineering 24(1-2): 51-80. doi: 10.1016/0378-3839(94)90026-4.

Ting, F.C.K. and Kirby, J.T., 1995. Dynamics of surf-zone turbulence in a strong plunging breaker. Coastal Engineering 24(3-4), 177-204.

van der A, D. A., van der Zanden, J., O'Donoghue, T., Hurther, D., Caceres, I., McLelland, S.J. and Ribberink, J.S., 2017. Large-scale laboratory study of breaking wave hydrodynamics over a fixed bar. Journal of Geophysical Research: Oceans, 122, 3287–3310. https://doi.org/10.1002/2016jc012072

Van der Zanden, J., Fernandez-Mora, A., Van der A, D.A., Hurther, D., Caceres, I., O'Donoghue, T., and Ribberink, J.S., 2017b. Inclusion of wave breaking turbulence in reference concentration models. Proceedings of Coastal Dynamics 2017. Helsingor, Denmark. 14, 629-641.

Van der Zanden, J., Van der A, D.A., Hurther, D., Caceres, I., O'Donoghue, T., and Ribberink, J.S., 2016. Near-bed hydrodynamics and turbulence below a large-scale plunging breaking wave over a mobile barred bed profile. Journal of Geophysical Research: Oceans, 121(8), 6482-6506.

Van der Zanden, J., Van der A, D.A., Hurther, D., Caceres, I., O'Donoghue, T., and Ribberink, J.S. 2017a. Suspended sediment transport around a large-scale laboratory breaker bar. Coastal Engineering, 125, 51–69. https://doi.org/10.1016/j.coastaleng.2017.03.007

Van der Zanden, J., Van der A, D.A., Cáceres, I., Hurther, D., McLelland, S.J., Ribberink, J.S. and O'Donoghue, T., 2018. Near-bed turbulent kinetic energy budget under a large-scale plunging breaking wave over a fixed bar. Journal of Geophysical Research: Oceans, 123, 1429-1456. https://doi.org/10.1002/2017JC013411

Van Rijn, L.C., 1984. Sediment Transport, Part II: Suspended Load Transport. Journal of Hydraulic Engineering, 110(11), 1613-1641.

Van Rijn, L.C., 2007. Unified View of Sediment Transport by Currents and Waves. II: Suspended Transport. Journal of Hydraulic Engineering, 133(6), 668-689.

van Rijn, L.C., Ribberink, J.S., van der Werf, J., and Walstra, D.J.R., 2013. Coastal sediment dynamics: recent advances and future research needs. Journal of Hydraulic Research 51(5): 475-493. doi: 10.1080/00221686.2013.849297.

Voulgaris, G. and Collins, M.B., 2000. Sediment resuspension on beaches: response to breaking waves. Marine Geology 167, 167-187.

Yoon, H.D., and Cox, D.T., 2010. Large-scale laboratory observations of wave breaking turbulence over an evolving beach. Journal of Geophysical Research: Oceans 115(C10).

Yoon, H.D., Cox, D.T. and Mori, N., 2015. Parameterization of time-averaged suspended sediment concentration in the nearshore. Water 7(11), 6228-6243.